Sonawane Shirish H (Orcid ID: 0000-0002-3201-6731)

Cu(II) ions removal from wastewater using starch nanoparticles (SNPs): An Eco-sustainable approach

Vikas S Hakke[1], Vividha K Landge[1], Shirish H Sonawane*[1], G Uday Bhaskar Babu[1], Sivakumar Manickam[2], Grzegorz Boczkaj[3,4]

[1]Department of Chemical Engineering, National Institute of Technology Warangal, Warangal 506004, TS, India.

[2]Petroleum and Chemical Engineering, Faculty of Engineering, Universiti Teknologi Brunei, Bandar Seri, Begawan, BE1410, Brunei Darussalam, Brunei.

[3]Department of Sanitary Engineering, Faculty of Civil and Environmental Engineering, Gdansk University of Technology, Poland.

[4] EkoTech Center, Gdansk University of Technology, G. Narutowicza St. 11/12, 80-233 Gdansk, Poland.

***Correspondence:**

Email: shirish@nitw.ac.in; Ph: +91-870-2468626

Funding Information

Prof. Shirish H. Sonawane acknowledges this research work to the Department of Science and Technology, Technology Mission Division, Government of India for providing financial assistance through the grant number DST/TMD/EWO/2K19/EWFH/2019/111(C).

Abstract

The complex structured starch particles were reduced to the nanoscale size range through hydrolysis utilizing low concentration acid assisted with ultrasound irradiation. The synthesized starch nanoparticles (SNPs) were characterized by TEM, FTIR, and XRD techniques. The synthesized SNPs possessed surface activated entities, as many cationic functional groups were confirmed through the FTIR spectrum. Also, these SNPs were effectively utilized to separate heavy Cu metal ions from the synthetic ion solution. The SNPs were characterized using FESEM, XPS and BET for the surface modification after the adsorption process. The weak electrostatic interaction between the SNP surface and Cu ion was confirmed from the XPS spectrum and energy dispersive X-ray spectroscopy. The maximum efficiency of Cu ions removal was about 93% at an optimal pH 5 and 25 mg/mL dosage. The adsorption equilibrium was obtained in 60 min. The nitrogen isotherm BET analysis of SNPs after adsorption shows a higher specific surface area of 18.552 m^2/g, attributed to the interaction and presence of Cu ions on the SNP surface. The process feasibility was validated by the Langmuir isotherm model. The process exhibits pseudo-second-order adsorption kinetics and follows the Langmuir isotherm. The R_L predicted by the Langmuir isotherm mechanism is 0.017, implying favorable adsorption. The process is reproducible and allows to separate heavy metal ions from the wastewater through bio-sorption effectively.

KEYWORDS: Bio-sorption, Ultrasound, Starch, Nanoparticles, Copper, Wastewater, Treatment.

1. Introduction

A continuous increase in product demand has resulted in the rapid growth of industrialization. The increasing industrialization causes various pollutants in the environment; however, it satisfies the product demand at the cost of various industrial practices[1,2]. The technology development in converting raw to the final product is still not up to the mark. Even under the current conditions, industrial practices cannot convert 100% raw materials into the final desired products. Thus, some unconverted or undesired product is always expected from each industry. These undesired products illustrate critical adverse effects on the surroundings. Hence, intense studies are needed to minimize such undesired products. Under the current environmental situation, unwanted products such as SOx, NOx, volatile organic compounds (VOCs), metal oxides, and heavy metal particles are categorized under high alert. Many industries nowadays create huge volumes of trash, including organic and inorganic substances that are poisonous and carcinogenic[3,4]. Particular attention must be paid to the presence of metal ions in aquatic environments. The hazardous qualities of these non-degradable ions are revealed when the amount of wastage dumped in the environment surpasses the safety threshold. It has become very important to extract heavy metals from industrial waste and natural water sources as these metals can harm the ecosystem and living things. These heavy metals in the industrial effluent arise from mining and refining ores[5]. The metal ions such as Pb(II)[6], As(III)[7], Cd(II), and Cr(VI)[8] are commonly found in industrial waste from tanneries, batteries, and paper mills[9], and are responsible for serious issues in the environment.

The industrial discharge containing the heaviest metal ions causes severe damage to the ecosystem. The various heavy metal ions (cation or anion) accumulate in the surroundings due to their higher ability to react with other substances. Cu and Ni are the most common heavy metals in water. Over time, Cu might cause damage to proteins, lipids, DNA, and organs, including the liver, kidneys and pancreas. Cu removal must be effective and affordable. The reported methods for the separation of Cu(II) from the wastewater are coagulation and precipitation[10], chemical precipitation[11], microfiltration membrane[12], reverse osmosis, adsorption[13], ion exchange[14] and most recent advanced oxidation processes [15]. These methods can effectively remove Cu(II) from the suspension. However, these methods are not cost effective and energy inefficient and laborious processes. While, the adsorption using natural resources (biosorbents) such as cellulose-complex[16], ground nutshell[9], pumpkin husk[17], calcined animal bone[18], and natural kaolinite clay[19] were found to be effective for the extraction of Cu(II) from the wastewater. Though these adsorbents effectively pull out toxic

Cu(II) from wastewater, the poor mechanical strength and rigidity, lower surface area limit their applicability[20].

The synthetic and natural adsorbents are explored in the adsorption processes[21]. Biosorbents have been effectively exploited to extract heavy metals from wastewater in recent years. The surface modification process for the biosorbents is much easier. The availability of raw biosorbents, economic value, and process efficacy make them suitable alternatives to chemical sorbents[22]. The conventional methods are expensive compared to the efficiency of removing the metal ions. The lower efficiency of the conventional methods is due to the higher concentration of heavy metal ions (10-100 mg/L). Also, the adsorption process is beneficial for large scale applications[23]. Notably, the natural adsorbent shows effective enhancement in removing pollutants as well their massive presence in nature compared to the chemical adsorbents[24]. Wang et al.[25] explored using nanomaterials as adsorbents. A proliferation in the surface area in the nanoscale of the adsorbent makes it more beneficial for removing heavy metals from the suspension. The nanomaterials show Brownian movement in the solution; thus, the wastewater has a higher mixing rate, reducing energy losses during mass transfer and positive flux between the adsorbent and heavy metal surface. The higher removal efficacy was found when the adsorbents were in the nanoscale[26].

He et al.[27] developed a lead-ion-imprinted magnetic biosorbent to remove Pb(II). They found that the developed nano-biosorbent showed higher sensitivity even when the suspension had the lowest concentration of Pb(II). Further, Celekli et al.[17] explored the pumpkin husk's Cu(II) adsorption capacity. They have reported the removal of Cu from suspension using the surface-modified (by KOH) pumpkin husk with maximum sorption of 73 mg/g. It exhibits the efficient application of biosorbent to remove Cu metal ions from the suspension. The dried orange peels were exploited to remove cupric ions from the waste, as demonstrated by Kumar et al.[28]. They noted that the monolayer adsorption of cupric ions was favourable during biosorption and the maximum cupric ions separation from the dried orange peels was 33.99 mg/g.

Starch is abundantly found in the agricultural outcome and even in agro wastes were optimistically employed in different applications. Starch granules are low-cost, and environmentally acceptable biomaterial. Agricultural waste products are now the most complex structures and concern for many decades[29]. Adsorption is important as it could remove hazardous contaminants from wastewaters. Thus, low-cost, readily accessible materials

that can adsorb Cu(II) are required. The biosorbents such as potato peels[30], fly ash[31], shell powder from groundnut[32], sesame straw[33], and coconut[34] have been reported in the literature. Acid or base treatment achieved the surface activation of potato peels and fly ash. These surface modified biosorbents showed high efficacy toward the adsorption of Cu from the suspension[14,35]. An innovative nanocomposite adsorbent made of Schiff base ligands was used to remove copper (Cu(II)) ions from wastewater[36].

In recent years, the synthesis and functionalisation of starch using nitrogen doping[37], acid treatment[38], alkaline treatment[39] to enhance the surface activity to efficiently remove Cu(II) ions from wastewater[40] have been reported. The novelty of the present work is that the produced SNPs do not require any functionalisation to pull Cu(II) ions from the solution. The SNPs are stable in the suspension. The starch granules are converted to nanosize through the hybrid acid hydrolysis method. The optimisation of the method was achieved with a series of experiments. The size of the resultant SNPs was confirmed from the TEM analysis. The as-prepared SNPs were used to remove Cu(II) metal ions from the solution. The mechanism and kinetics of the adsorption were studied, and the extraction efficacy of Cu(II) metal ions was examined. The copper removal from the solution using SNPs as bio-sorbents is discussed. The effect of operating conditions such as variations in the pH of suspension, initial concentration of Cu(II) in the suspension has been analysed. The process is novel as the synthesized SNPs did not require surface modification for the metal ion removal. The synthesized SNPs possessed the functional group, enhancing the affinity of Cu(II) ions towards the SNPs surface. The synthesized SNPs produced a stable colloidal suspension which was confirmed by measuring the zeta potential. The maximum efficiency of 93% for Cu(II) metal ions was noted using SNPs as biosorbent.

2. Material and Methods

2.1 Materials

The corn starch granules were purchased from Sigma Aldrich, India. The laboratory-grade sulfuric acid (H_2SO_4) and copper sulphate ($CuSO_4 \cdot 5H_2O$) were purchased from Thermo Fisher Scientific, India.

2.2 Synthesis and optimization of SNPs

The ultrasound-assisted acid hydrolysis was used to synthesize SNPs. For this, starch granules with the initial average granular size ranging from 5 to 9 μm, received from Sigma Aldrich,

were used to reduce to the nanoscale size. The variations in the acid concentration were examined with constant power input and irradiation time to obtain an optimal acid concentration for the minimal size of the starch granules. The desired acid concentration was prepared using the stock solution of H_2SO_4 (0.5 M).

The ultrasound-assisted hybrid acid hydrolysis was carried out at constant power input and irradiation time. Initially, 5 g corn starch was dissolved in 250 mL H_2SO_4 solution (0.5 M). The solution was then subjected to ultrasound irradiation with an input power of 120 W and a frequency of 20 kHz (Ultrasonic probe sonicator 12/20 VR, Dakshin, Mumbai, India) for 45 min (5 s On and 3 s Off for each 8 s cycle). The solution temperature was maintained below 50 ^oC by immersing the vessel in the cooling bath during all the cycles of ultrasound irradiation. The digital thermometer (TA Instruments, USA) was employed to check the solution temperature during the operation. The separation of surface activated SNPs from the suspension was achieved using centrifugation followed by vacuum drying. The experiments were carried out in three sets for consistency.

2.3. Preparation of synthetic Cu(II) ion solution

Cu(II) salt was dissolved in deionized water to obtain the stock solution. 24.97 g $CuSO_4.5H_2O$ was dissolved in 1000 ml of deionized water to produce a stock solution of fixed concentration[28]. The working solutions with initial Cu concentrations varied from 5 mg/L to 35 mg/L and were attained by diluting the stock suspension. The solution pH was attained to the required value using an appropriate buffer solution (acidic buffer with pH 2, 3, 4, 5 and 6; basic buffer of pH 8). The resultant stock solutions were sealed in an airtight container and kept in a refrigerator.

2.4. Experimental procedure and method of analysis

The adsorption experiments were performed in a batch mode with a working volume of 200 mL using a 250 mL flask. The primary aim is to find the concentration gradient of Cu(II) ions in the suspension through the adsorption process. The concentration gradient is the number of Cu(II) ions removed from the solution. The fixed quantity of SNPs adsorbent was added into a 200 mL suspension of known Cu(II) ion concentration. The initial and final Cu(II) ion concentrations in the suspension were determined via a UV-visible spectrophotometer at 434 nm[40]. The adsorption capacity of SNP was estimated using the following Eq.1.

$$Q_{Ad} = (C_{Cu_0} - C_{Cu_e})\frac{V}{m} \qquad (1)$$

Where C_{Cu_0} and C_{Cu_e} denote the copper metal concentration at the start and equilibrium, correspondingly. V represents the solution volume, and m denotes the adsorbent mass. Q_{Ad} is the adsorption capacity of SNP in mg/g. The comparative extraction of Cu(II) from the suspension was calculated using Eq. 2.

$$Cu\ removal\ (\%) = \frac{(C_{Cu_0} - C_{Cu_e})}{C_{Cu_0}} \times 100 \qquad (2)$$

Copper removal efficiency (%) was calculated and compared under different operating conditions. The variation in the initial concentration of Cu(II) in the suspension, pH, and the added amount of SNPs were considered. The optimal conditions to achieve the maximum Cu(II) adsorption from the suspension were noted.

2.5. Characterization of biosorbent

The dry powder of SNPs was kept in a desiccator to avoid moisture influence. To prepare a synthetic Cu(II) stock solution, an appropriate amount of copper sulphate ($CuSO_4 \cdot 5H_2O$) was dissolved in deionized water. The solution pH was maintained in an acidic regime to generate the driving force for adsorption. The synthesized SNPs were introduced to the stock solution with the known initial Cu(II) ion concentration. After reaching the equilibrium, the SNP/Cu complex sediments were formed in the solution. Then, the solution was centrifuged (Eppendorf® Centrifuge, 5430R, Germany) at 6500 rpm for 15 min at 10 ºC to separate the SNP/Cu complex from the solution. The SNP-Cu complex was then vacuum dried at 40 ºC and stored in a desiccator until further characterization.

FTIR was used to determine the existence of active functional groups in the SNPs. TEM (transmission electron microscopy, Vitrobot Mark IV 200 kV, USA) was employed to examine the SNPs adsorbent capacity to metal particles. The Cu adsorption on the starch surface was confirmed from the X-ray fluorescence (XRF) (ED-XRF) (EPSILON-1 PANalytical, Netherlands) diffraction. The biosorbent was analyzed for metal components through XRF. The effect of pH, initial concentration of Cu, and the SNPs dosage on the overall removal efficiency was investigated. The SNPs before and after Cu adsorption were characterized by XRD (PANalytical XPERT-PRO, Netherlands) to find crystallinity changes due to the sorption of Cu on the SNPs granules. XRD was performed at 30 mA and 40 kV with a scan range (2θ) of 10 to 80º at a scan rate of 0.02 s^{-1}. The shift in the diffraction pattern could be because of the functional group attachment with the Cu ions from the suspension. The field emission scanning electron microscope (FE-SEM) (ZEISS Sigma 500 VP, Germany) and X-ray

photoelectron spectroscopy (XPS) (PHI Versaprobe III, Canada) were used to analyze the surface modification and binding energy variations in the SNP before and after Cu adsorption. The zeta potential was measured at the equilibrium pH of the suspension using a Malvern zetameter (Zetasizer Nano Z, PANalytical, Netherlands). The surface area analysis was carried out using Brunauer–Emmet–Teller (BET) analysis with nitrogen adsorption isotherm employing surface analyzer Belsorp mini II (Microtrac, Japan).

3. Results and Discussion

3.1 Characterization of SNPs

The hybrid acid hydrolysis assisted with ultrasound led to form SNPs and were characterized using TEM to obtain their exact morphology. As shown in Fig. 1a, SNPs exhibit an oval shape at the magnification scale of 50 nm. Fig. 1a also shows the multilayer occupancy of the granular SNPs. The average particle size of SNPs ranged from 50 to 80 nm. The intensified hybrid acid hydrolysis and ultrasound irradiation significantly affect the particle size reduction. The conventional acid hydrolysis process proved efficient with limited particle size distribution and 36% yield [41].

Fig. 1 TEM of SNPs (a) before adsorption (b) after adsorption

This demonstrates the efficiency of ultrasound to aid the acid hydrolysis of starch compared to the conventional acid hydrolysis reported by Wang and Copeland[42]. This could be explained by the overall effect generated during the ultrasound process. The chemical and mechanical phenomena observed during sonication play a significant role in achieving a lower particle size distribution. The mechanical shock waves induced during the collision of cavities generate intensified local turbulence responsible for the higher mass transfer rate of acid molecules towards the starch surface. In addition, it also affects the sonolysis of water, producing hydroxyl radicals and their intense mixing and diffusion in the solution, increasing the hydrolysis rate[43].

The amorphous part of the starch granules reacts quickly with the acid. These amylopectin molecules in the amorphous part of starch granule hydrate during the reaction with acid. The hydrated amylopectin could behave as a liquid crystalline polymer[44]. However, the crystalline segment of starch granules shows high resistance to hydrolysis. The ultrasound irradiation during the acid hydrolysis assists in keeping the particles in the suspension. A higher surface

area is available for the interaction with the surrounding acid when the starch granules are suspended, resulting in a higher hydrolysis rate.

Fig. 2 shows the XRD of starch granules after the hybrid hydrolysis process with different acid concentrations. It clearly shows a much higher SNPs crystallinity than the initial granules; these results are similar to the observations reported by Haaj et al.[44].

Fig. 2 X-ray diffraction spectra of SNPs synthesized using H_2SO_4 of different concentrations (0.25 M, 0.5 M, and 1 M).

The consistent A-type crystalline packing of SNP granules was observed with all the acid concentration interactions (Fig. 2). However, the peak becomes narrower with the changes in acid concentration. Intense peaks were observed at 15º, 16.96º, 18.1º and 23º. The optimization of acid concentration was examined, and it has been noted that acid concentration plays an important role in synthesizing SNPs with lower size distribution. The produced SNPs with different acid concentrations show different particle size distributions and variations in the morphology of the produced SNPs. The SNPs synthesized with lower acid concentration show lower particle size distribution than the higher concentration. Most of the anionic functional groups directly interact with SNPs at higher acid concentrations, as illustrated in Fig. 3(a). At higher acid concentrations, the hydrolysis rate is much higher than at lower concentrations; more sulfonic groups occupy the surface of the synthesized SNPs. The higher number of sulfonic groups on the surface makes SNPs unstable in the suspension. This instability of SNPs in the high acid concentration suspension could be the major reason for agglomeration. The agglomerated structure has a lower surface area exposed to acid hydrolysis, reducing the hydrolysis rate even at higher acid concentrations[45].

Fig. 3 (a) FTIR spectrum (b) Zeta potential of the synthesized SNPs granules with different acid concentrations.

The self-agglomeration could continue till equilibrium was achieved[46]. The balancing force between the functional group ultimately terminates the agglomeration process, resulting in the higher particle size distribution of SNPs. The functional group activity is limited at lower acid concentrations due to the high concentration of hydrogen ions present in the surroundings. The availability of the higher number of hydrogen ions at lower pH makes the synthesized SNPs more stable. At lower concentrations, SNPs could behave like individual entities. Several forces such as drag force, gravitational force, the intermolecular force of interactions could

simultaneously act on the surface of SNPs. The shear force distribution on the surface is uniform at lower acid concentrations. The sedimentation rate is much higher than the resuspension rate at higher concentrations. However, the resuspension rate is higher at a lower concentration than the sedimentation rate[47]. The zeta potential of the SNP suspension is illustrated in Fig. 3b, indicating that the stability of the SNPs synthesized using different acid concentrations is different in the suspension. The difference in the surface charges of SNPs is due to changes in the acid concentration. Also, the changes in the surface charges lead to different size distributions. The variation in the morphology is due to the agglomeration rate of SNPs.

The intensification of the acid hydrolysis process is observed under ultrasound irradiation. The process required 50 min to reduce the starch granules from the micron-scale (5-9 μm) to the nanoscale (50-80 nm). The ultrasound irradiation generates cavities as intensifying sound vibrations interact with the suspension. The life span of these generated cavities is very short, during which the nucleation, growth and collapse occur within a fraction of time. The collapse of cavities is random, which assists in breaking the starch granules so that acid could impinge into the granules. This is why hydrolysis is faster than conventional processes. The amorphous segment of the starch granules interacts first with acid, followed by the crystalline portion. The crystallinity of the synthesized starch granules is much higher than the initial starch granules. Our earlier study reported an increase in the crystallinity by 50 fold[48]. The experimental investigation also shows that the synthesized SNPs are more stable at a lower acid concentration (0.05 M) with a smaller particle size of 50 nm. As the acid concentration increases, the stability of nanoparticles reduces due to the synergetic effect of the functional group associated with the granular surface, and the agglomeration rate enhances. This leads to a larger particle size in the suspension. The yield in this process is 36 % higher than the earlier reported work[44,49].

3.2 TEM and FESEM of the SNPs before and after adsorption

As discussed in section 3.1, the transmission electron microscopical images show particle size differences in Figs 1 (a) and (b). The difference in the particle size was due to the presence of Cu ions on the surface after the adsorption. Fig. 1 (b) illustrates the larger particle size compared to the SNP in Fig 1 (a). The Cu ions present on the SNP surface are stable. The field emission scanning microscopy gives a clear morphological difference between the SNP before and after adsorption. The Cu ions interact with the sulphonic functional group on the surface

of SNP. This interaction can be confirmed from the energy-dispersive X-ray spectroscopy (EDS) observations. The weak chemical bond between the sulfonic group and Cu(II) metal ions leads to agglomeration in the surface-active SNPs. The XRF and energy dispersive X-ray spectroscopy (EDS) spectra confirm that the sediments separated from the stock solution after 60 min contained starch as well as Cu metal ion.

Fig. 4 FE-SEM of SNPs before (a) and after (b) the adsorption process, the corresponding energy-dispersive X-ray spectroscopy (EDS) for SNPs before (c) and after (d) adsorption.

The FESEM characterization was carried out to obtain information about the surface morphology of both the SNPs before and after the adsorption of Cu. The FESEM of the SNPs before and after the adsorption process is illustrated in Fig. 4, along with corresponding energy-dispersive X-ray spectroscopy (EDS) observations. The microscopic images in Fig. 4 (a, b) confirm the surface attachment of Cu ions on the SNPs granules. The EDS confirms the presence of sulphur from the sulfonic functional group on the surface of SNPs before the adsorption process, which was overcome due to its interaction with the Cu ions during the adsorption process. The presence of Cu ions in different oxidation states at different energies on the SNPs surface after the adsorption process indicates its electrostatic interaction with the SNPs surface. Fig. 4(b) shows that SNPs-Cu agglomerates are more likely after drying than SNPs adsorbent, possibly due to intermolecular interactions between Cu ions in the complex[26].

3.3 Brunauer-Emmett-Teller (BET) Characterization of SNPs before and after adsorption

Fig. 5 N_2 adsorption/desorption isotherms for the SNPs before and after adsorption of Cu(II)

The nitrogen gas adsorption isotherms are depicted in Fig. 5, exhibiting similarities with the typical IV type adsorption behavior[16]. Also, the N_2 isotherms exhibit a well-known sharp modulation of adsorption/desorption limbs where the adsorption branches are significantly shifted toward lower relative pressure (P/P_0). Based on the N_2 isothermal results, the mesoporous SNPs adsorbent illustrates appreciable specific surface area, mesoporous volume (V_m), and tunable mesoporous diameters (D_m). The SNPs show a higher surface area after the adsorption process due to the adsorption of Cu on the surface.

3.4 FTIR analysis of SNPs

FTIR is an essential tool to examine the functional groups capable of adsorbing Cu(II) metal ions. The sulphonic group (-$OHSO_2$) on the SNPs surface was confirmed through a band at 1019 cm^{-1}.

Fig. 6 Comparative Fourier transform infrared (FTIR) spectra of SNPs before and after adsorption.

The broad band at 3329 cm^{-1} illustrates the stretching vibrations of the hydroxyl group. The stretching energy of the hydroxyl group indicates the adsorption of moisture by the SNPs during analysis. The carbonyl groups on the starch surface could be found at 1075 cm^{-1}. The stretching of the bond between C-O was observed due to the vibration in the range of 1636-1382 cm^{-1}. Fig. 6 shows the FTIR spectrum of SNPs before and after Cu(II) adsorption, illustrating a shift in the intensity of the -OH and carbonyl bands after sorption, demonstrating their participation in adsorption. Surface -OH group is one of the active functional groups responsible for Cu(II) adsorption as the wavenumber shifts from 1650 cm^{-1} to 1729 cm^{-1}. The characteristic sulphone (S=O) stretching vibrations band for SNPs at 447 cm^{-1} disappears significantly after the adsorption of Cu(II). This indicates its involvement in the adsorption of Cu ions. The band at 629 cm^{-1} reveals the presence of a -Cu- bond associated with the surface of SNPs. The characteristic band of the sulphonyl (-S=O-) functional group present at 547 cm^{-1} in SNPs shifted to 629 cm^{-1} after adsorption. This shift confirms that it is strongly involved in the adsorption of Cu(II) ions through bonds from the hydroxyl functional group. The band shift between 600 and 750 cm^{-1} in the SNPs after adsorption implies the presence of Cu metal ions. The -Cu bond energy is significantly observed between 550 and 750 cm^{-1}.

3.5 XPS and XRF spectra of SNPs before and after adsorption

X-ray photoelectron spectroscopy (XPS) is used for the chemical analysis of SNPs before and after adsorption. The surface chemical species analysis for the starch granules before and after the adsorption process for the depth of 5 nm was achieved. The surface depth analysis for the SNPs before and after adsorption was also achieved. The X-ray photoelectron spectrometer used characteristic Al Kα radiation as an excitation source and a constant pass energy of 40 eV. The binding energy (BE) of C 1s was shifted to 284.6 eV as an internal reference. In Fig. 7, the XPS inspection spectra of SNPs, SNPs-Cu and high-resolution XPS spectra of C1s, O1s and S1s have been shown for the changes in surface elements and their bond energies. The

main elements in the SNPs adsorbent are C1s, O1s and S1s. The hydroxyl and sulphonic functional groups on the surface of SNPs could be confirmed (Fig (b), (c) and (d)). After Cu ion adsorption on the surface of SNPs, Cu appears in the XPS spectrum of SNPs-Cu nanocomposite. Further, the chemical environment changes of the surface elements were analyzed by the high-resolution spectra of C1s, O1s and Cu 1s in XPS.

In the spectrum of C1s (Fig. 7(b)), the starch nanoparticles present a single peak of 284.6 eV, corresponding to stable carbon bonds. These are attributed to the of C1s in the glucose monomers. The new peaks at 284.72 eV and 282.99 eV show the interaction of C1s with the Cu ions after adsorption. In the spectrum of O 1s (Fig. 7(c)), the peak at 531.62 eV can be attributed to the C-O bond, unaffected by the adsorption process. The variation in the intensity of the peak is attributed to OH radical interactions at the surface with the Cu ions and surroundings.

Fig. 7 (a) High-resolution XPS spectrum of the surface activated SNPs before and after adsorption; (b) for C1s (c) for O1s, and (d) for S1s.

The new linkages develop between hydroxyl or carboxyl groups on the surface of starch nanoparticles due to acid hydrolysis during the size reduction increasing the intensity at 531.62 eV. The sulfonic functional group interaction with the Cu ions is illustrated in Fig. 7(d) for all S 1s at 167.29 eV. The intensity variation is due to the electrostatic interaction of S 1s. The new peaks at 934.74 eV, 572.03 eV, and 77.29 eV could be attributed to Cu (II), Cu and Cu(III) interactions of Cu with the SNPs surface. The peak strength of S 1s is decreased after Cu(II) adsorption, indicating that Cu(II) is involved in the adsorption process.

XRF is an elemental analysis method that detects the presence of specific elements using secondary X-rays generated by individual atoms. The XRF spectrum for the SNPs after the adsorption process is illustrated in Fig. 8.

Fig. 8 XRF spectrum of the surface activated SNPs after adsorption.

The Cu component in the spectrum is significantly higher than other metal components. Other metal components are due to the contamination of impurities during sample handling. The adsorption of Cu on the SNPs surface is prominent due to the interaction with the hydroxyl

group. This is why the concentration of Cu on the surface of SNPs is more prominent. Cu metal ions on the SNPs surface are seen in Fig. 8, where they attract surfaces more strongly than other metal ions[50].

3.6 Zeta potential of SNPs after adsorption

Fig. 9 Zeta potential of SNPs after adsorption

Fig. 9 illustrates the zeta potential of SNPs-Cu after adsorption. After 60 min of adsorption equilibrium, the dried SNPs were analyzed for the potential charges along the surfaces. The higher negative charge (-68 mV) of the colloidal solution of SNP-Cu shows higher stability. The additional potential in SNP granules after the adsorption confirms the presence of attached Cu ions on the surface.

3.7 XRD of SNPs before and after adsorption

The SNPs possess a semi-crystalline structure (Fig. 10). Ultrasonic cavitation destroys the natural starch particles, elucidating a high impact of the resultant cavities collapse. The critical peak of Cu is predominant on the surface of starch by comparing the SNPs before and after adsorption. The XRD diffraction of SNPs-Cu shows significant variations. The prominent peak of Cu is found at 36.65º and 42.47º. The diffraction supports the adsorption of Cu on the surface of SNPs.

Fig. 10 XRD spectrum of SNPs before and after adsorption compared with Cu NPs.

3.8 Effect of adsorbent dosage and pH variation on the removal efficiency of Cu

Adsorption is a surface phenomenon. The higher quantity of SNPs gives a larger surface area for the adsorption process. At the fixed initial concentration, the effect of dosage on the adsorption efficiency of Cu(II) metal ions was studied. The adsorption efficacy depends upon the available surface area on SNPs. As the dosage of SNPs increases, adsorption sites and hence the effective surface area available for adsorption increases several folds, leading to higher extraction efficiency of Cu(II) ions from the suspension. However, the increase in removal efficiency was up to a certain critical limit with increasing dosage. After this critical limit, the actual enhancement in Cu(II) adsorption with respect to the increasing amount of SNPs was much lower. Thus, a further increase in the dosage after the critical limit does not significantly enhance the removal efficiency of SNPs. This phenomenon could be ascribed to the occupancy of all the active sites on the surface of SNPs followed by equilibrium achievement in the

multilayer formation. The Cu(II) ions might be assembled in a multilayer on the SNPs surface. The progress of such a multilayer formation could depend on the adsorption forces arising from SNPs. At the critical dosage of SNPs (25 mg/mL), the strength of adsorption forces could be balanced by the maximum number of Cu(II) molecules. Due to this, after the critical dosage limit, the actual Cu(II) ion adsorption rate is much lower, and the actual Cu(II) absorbed on the SNPs is much lower. Thus, excess dosage after the critical limit is not economical. Another reason for the lower adsorption rate might be the agglomeration of SNPs. The intermolecular interaction between SNPs molecules will be higher at a higher dosage.

Fig. 11 Effect of a) SNPs dosage b) pH on the removal efficiency of Cu(II) ions.

Such a higher interaction may lead to agglomeration of SNPs which diminishes the overall available surface active sites for adsorption. As the accessibility to the number of active sites reduces at a higher dosage, the removal efficacy after a critical limit is lower.

Thus, the addition of SNPs after the critical dosage does not have any significance. The uniform mixing of SNPs directly affects the removal of Cu(II) ions. The interaction of Cu(II) ions with SNPs enhances the adsorption rate. The removal efficiency of Cu(II) is almost constant beyond the optimal dosage of SNPs. As shown in Fig. 11 (a), the maximum removal of 93 % was obtained at a 25 mg/mL dosage. A similar reduction in the adsorption capacity of Cu(II) ions has been reported by Kumar et al.[28]. Additionally, the results indicate that the critical limit of the dose may not be constant for all the adsorbents, which depends on the surface area of the adsorbent and the number of adsorbates. Intermolecular forces are crucial in determining the amount of critical dose. The adsorption of Cu(II) ions on the adsorbent surface of SNPs is due to the interaction between the charged surface. The surface charges on the SNPs and Cu(II) metal ions play a significant role in the overall removal efficiency. A change in the pH varies the concentration of H^+ ions in the suspension, which is in direct contact with both the adsorbent as well as the adsorbate. The effect of pH on the surface charges of the absorbent and adsorbate during the adsorption process was studied by varying pH values. The removal efficiency of Cu(II) ions on the surface of SNPs was studied in the range of pH from 2 to 8.

Fig. 11 (b) illustrates the removal efficiency of Cu(II) ions with changes in pH. At an optimal pH of 5, the maximum removal efficiency of 93% was achieved. Also, the removal efficiency increases with an increase in the pH from 2 to 5. The lower is the pH value; the larger is the number of H^+ ions present in the suspension. This higher number of H^+ ions directly affects the affinity of Cu(II) towards the surface of the SNPs adsorbent. In comparison to Cu(II), positively

charged hydrogen ions interact more strongly with the active sites of SNPs at lower pH values. This results in an overall lower adsorption efficiency of Cu(II) ions. However, with an increasing pH value of suspension, the number of H^+ ions decreases in the suspension, increasing SNPs adsorption efficiency for Cu(II). The increase in Cu(II) removal efficiency was noticed up to the optimal pH of the suspension. Similar results were observed by Kubra et al.[51] using functionalized lignin-based complex for the adsorption of Cu(II).

A further increase of pH above the optimum value decreases the Cu(II) removal efficacy of the as-produced SNPs. The higher pH suspension contains a higher concentration of HO^- ions, which interact with Cu(II) ions and results in a complex structure that includes forming a stable CuO structure in the suspension. CuO has a lower affinity for the active sites of the SNPs surface. As a result, the Cu(II) removal efficiency of as-produced SNPs at higher pH values is low. At a pH greater than 5, the removal efficacy of Cu (II) on the SNPs decreases. The optimal pH depends on the surface interactions between the adsorbent and the targeted adsorbate.

3.9 Effect of initial concentration of Cu ions in solution

The interaction between the active sites on the surface of the adsorbent and the moving Cu(II) ions in the suspension affects the adsorption mechanism. The impact of the initial concentration of Cu(II) ions on the available active sites of the adsorbent is significant. The effect of initial Cu(II) ions on the removal efficacy was studied with a fixed amount of SNPs. The activation sites on the adsorbent are constant at the constant amount of SNPs. The interaction between active sites of SNPs and Cu(II) ions separates Cu(II) ions from the suspension. Thus, the limiting component of the process is the availability of active sites on the SNPs surface. With the increase in the initial concentration, the removal efficiency of Cu(II) ions increases, which is up to an optimal concentration. The removal efficiency decreased drastically with an increase in the initial concentration. The concentration changes were observed from 5 to 35 mg/mL of cupric ions, keeping the pH and the amount of SNPs constant. Fig. 12 shows the removal efficacy of cupric ions with an increase in the initial quantity of cupric ions per mL of suspension at constant pH (5) and SNPs loading (25 mg/mL). The volume of cupric ions present in the suspension illustrates the significant effect on the extraction efficiency of SNPs. At the volume fraction of Cu(II) ions in the suspension, the availability of active sites is higher; also, the binding affinity between the surface of the adsorbent and adsorbate is high. This results in a higher rate of adsorption of Cu(II) ions on the SNPs surface. The heat of adsorption released during adsorption is much lower than the heat of desorption, favorable for the higher adsorption rate. Thus, at a lower concentration, higher removal efficacy is observed.

Fig. 12 Effect of initial concentration of Cu(II) ions on the adsorption capacity of SNPs.

The decrease in the removal efficiency may occur due to the higher lateral interaction between adsorbate molecules. The lateral interactions between the adsorbate Cu(II) molecules involve higher energy exchanges through the Brownian motion, the force of attraction and repulsion, making them unstable on the surface of adsorbent SNPs. This increases the desorption rate compared to the adsorption rate of Cu(II) adsorbates on the surface of SNPs.

The formation of a monolayer on the active sites of SNPs was observed at higher initial concentrations of Cu(II) ions. The lateral interaction of Cu(II) ions in the suspension prevent further propagation of Cu(II) adsorption beyond the monolayer. The local mass transfer coefficient values of individual Cu(II) molecules are affected by lateral interaction at higher concentrations of Cu(II). This results in a lower rate of Cu (II) transfer from the suspension to the actual active site of the SNPs adsorbent. As a result, the removal efficiency of Cu(II) from the suspension is reduced. Thus, adsorption at a higher initial concentration of Cu(II) follows the Langmuir isotherm, reducing the removal efficacy of Cu(II) ions compared to its lower initial concentration.

3.10 Mechanism of Cu adsorption on SNPs

The mass transfer-driven adsorption involves the sedimentation of copper metal particles on the surface of SNPs. The interface interaction between the SNPs and Cu ions could be in two ways, one goes with bioaccumulation, and another is biosorption. The accumulation of Cu ions on the surface of SNP does not offer any physical or chemical interactions. However, Cu will be bounded with the physicochemical bond with the SNP surface in the biosorption. The possible adsorption mechanisms of metal ions onto biosorbents include physical adsorption, chemisorption, electrostatic interactions, hydrogen bonding, pi-pi interactions, and precipitation. The representation of a possible mechanism is illustrated in Fig. 13.

Fig. 13 Mechanism of the adsorption of Cu ions on the SNPs surface.

The FTIR analysis of SNPs confirms the presence of functional groups such as carbonyl, carboxyl, and hydroxyl groups on the surface of SNPs granules, which are most often negatively charged. Besides, the metal ions can be adsorbed onto the pores and cavities on the surface of SNPs. The microporous SNPs surface is verified with the BET analysis of SNPs before the adsorption process. The higher adsorption amount of N_2 molecules on the surface of

the SNPs-Cu cloud may be because of the higher pore density associated with the complex. The adsorption of Cu(II) ions from wastewater involve the diffusion of Cu(II) ions and their binding to the SNPs surface via electrostatic attractions[52,53]. It can be suggested that the electrostatic attractions between positively charged metal ions and the negatively charged functional groups of the SNPs could successfully promote the adsorption capacity. Other attractive forces, such as Van der Waal forces, hydrogen bonding, and concentration gradients, may be involved in Cu(II) ion adsorption on the surface of SNPs[39].

3.11 Adsorption kinetics

The adsorption process depends on the overall contact time between the adsorbent's surface and the number of adsorbates in the suspension. With a longer time, a higher quantity of Cu(II) ions could interact with the SNPs and hence a higher separation. The adsorption kinetics shows a certain optimal value where the desorption balances all the adsorptive forces from the SNPs granules. No further significant Cu (II) ion adsorption on the SNPs surface. This optimum is the equilibrium condition, and the time to reach this condition is the minimum time or equilibrium time[54].

Fig. 14 Effect of contact time on the removal efficiency of Cu(II) ions from the solution.

In the present work, the SNPs obtained higher Cu ion removal efficiency in a short equilibrium time of about 60 min. Table 1 shows various bioadsorbents for the removal of Cu ions from wastewater.

Table 1. Overview of the reported bio-adsorbents for the removal of Cu ions from wastewater.

Biosorbent used for adsorption	Sorbent	Maximum efficiency (mg/g)	Optimal conditions	Isotherm Validated	Mechanism	Ref.
Calcined animal bone	Zn (II) and Cu (II)	Zn(II) : 26.93 Cu(II): 22.98	pH: 4.5; Et: 180 min; D: 2-16 g/L; Ci: 100 mg/L	Pseudo-second order kinetics	Electrostatic attraction and surface adsorption	[18]

Calcite modification of agricultural waste (coconut biochar (CAL/BC))	Cu(II)	21.3	pH: 5.5; Et:100 min D: 0.05 g/L; Ci: 100 mg/L	Pseudo-second order model and Langmuir model	Monolayer chemisorption	[29]
Pectin based composite hydrogel derived from grapefruit peel	Cu(II)	80.6	pH: 6; Et: 100 min; D: 25 %; Ci: 100 mg/L	Pseudo-second order model and Langmuir model	Electrostatic attraction, ion exchange and physical adsorption	[55]
Gundelia Tournefortii	Cu(II)	38.8	pH: 3; Et: 50 min; D: 5 g/L; Ci: 200 mg/L	Pseudo-second order and Langmuir model	Weak electrostatic interaction	[56]
Green vegetable waste	Cu(II)	75	pH: 3.5; Et: 120 min; D: 0.6 g/L; Ci: 1.5 mg/L	Langmuir isotherm model and pseudo-second order reaction	Physical adsorption	[57]
low cost natural/agricultural waste biomasses	Cu(II)	75	pH: 6; Et: 180 min; D: 0.6 g/L; Ci: 25 mg/L	Dubinin-Radushkevich isotherm model Pseudo-second order model	Monolayer adsorption and physicochemical adsorption	[54]

SNP (present work)	Cu(II)	93	pH: 5; Et: 60 min; D: 25 mg/mL; Ci: 15 mg/L	Langmuir isotherm model and pseudo-second order reaction	Monolayer adsorption and physicochemical adsorption	

* Et: Equilibrium time (min); Ci: Initial concentration of adsorbate (mg/L); D: Dosage (g)

The kinetics of Cu(II) adsorption was studied with changes in the removal efficiency with respect to time. Fig. 14 illustrates the removal efficiency with respect to time. Two pseudo-first order and pseudo-second order kinetics were utilized to verify the adsorption kinetics.

The pseudo-first order adsorption kinetics was evaluated using the following Eq. 3.

$$\log(Q_e - Q_t) = \log(Q_e) - \frac{k_1}{2.303} t \quad (3)$$

Where k_1 is the constant. The graph of $\log(Q_e - Q_t)$ Vs t (Fig. 15 (a)) gives an overview of the pseudo-first- order adsorption kinetics. The overall linear regression value (R^2) for the pseudo-first order kinetics is 94 %. The intercept and slope of the regression were calculated, and then k_1 and intercept $\log(Q_e)$ were obtained.

Pseudo-second order adsorption kinetics was evaluated by the following Eq. 4.

$$\frac{t}{Q_t} = \frac{1}{k_2 (Q_e)^2} + \frac{1}{Q_e}(t) \quad (4)$$

Fig. 15 (b) illustrates the kinetics of $\frac{t}{Q_t}$ Vs t. The slope and intercept provide the values of second order, constant k_2 and the equilibrium quantity (Q_e) of Cu(II) ions adsorbed per gram of SNPs, respectively. The regression value of second order kinetics is 0.9873, higher than the pseudo-first order kinetics. These observations exhibit that the pseudo-second order adsorption kinetics is the more suitable for this adsorption[58].

Fig. 15 (a) Pseudo-first order adsorption kinetics (b) Pseudo-second order adsorption kinetics of Cu(II) ions on the surface of SNPs.

3.12 Adsorption isotherm

The basic operation principles for Cu(II) adsorption are the mass transfer and physicochemical interaction between adsorbate (Cu) and adsorbent (SNPs). The adsorption process could be understood through various isotherms. These isotherms are equilibrium correlations amongst the various process parameters. The isotherm helps to define the mechanism through which the progress of the adsorption process occurs. The Langmuir adsorption isotherm and Freundlich isotherm are commonly used primary mechanisms of the adsorption processes. The monolayer adsorption is associated with the Langmuir isotherm, whereas the multilayer adsorption isotherm validates the Freundlich isotherm. The quantitative distribution of adsorbate in the two distinguished phases as solid-phase adsorbent and liquid phase suspension at equilibrium conditions can be estimated using the isotherm. The monolayer formation of adsorbate on the adsorbent surface can be explained using the Langmuir isotherm. The number of active sites available for adsorption on the adsorbent surface will only be occupied by the equivalent number of adsorbates. The multilayer formation of adsorbate on the adsorbent surface is not considered by the Langmuir adsorption isotherm. The Langmuir isotherm should have been treated as an ideal condition for adsorption[56].

In comparison, the specialty of the isotherm is the value of R_L. The R_L calculated from the Langmuir isotherm verifies the feasibility of the adsorption process. If the value of R_L is greater than 1, the adsorption is not favorable; however, when $0<R_L<1$, the adsorption is favorable. The adsorption process is irreversible in the case of $R_L = 0$[59].

Fig. 16 (a) Langmuir adsorption mechanism (b) Freundlich isotherm mechanism.

The affinity of Cu(II) ions towards SNPs in the suspension was validated from these isotherms. Following equations of Langmuir isotherm (Eq. 5) and Freundlich isotherm (Eq. 6) were used to plot Fig. 16 (a) and 16 (b), respectively. The value of R_L is calculated from the slope and intercept of Fig. 16 (a) (Eq. 7).

$$Q_e = \frac{X}{M} = \frac{Q_{max} * b\, C}{1 + bC}$$

$$\frac{1}{X/M} = \frac{1}{Q_{max}} + \frac{1}{Q_{max} b}\ \frac{1}{C_t} \quad (5)$$

$$\log Q_e = \log K + \frac{1}{n} \log C \quad (6)$$

$$R_L = \frac{1}{1+bC_o} \quad (7)$$

Where b is the Langmuir constant, while K and n are the Freundlich constants for the adsorbent and adsorbate pair, respectively.

From the Langmuir isotherm, the value of R_L= 0.017 tends towards the irreversible behavior of the process. The R^2 value of the Langmuir isotherm is 98% which is higher than the value of the Freundlich isotherm. Thus, adsorption follows Langmuir adsorption behavior. The maximum value of Cu(II) separated from the solution is 43 mg/g of SNPs, indicating good applicability of the developed adsorbent for real case scenarios [56].

4. Conclusions

SNPs were synthesized through the robust ultrasound assisted acid hydrolysis process. By process optimization, the synthesized SNPs show smaller particle size distribution at a low acid concentration (0.25 M) (50-80 nm). As-synthesized SNPs are the surface activated entities, and the anionic functional groups are present on the SNPs surface. These SNP were utilized for the extraction of cupric ions. The process was favorable and confirmed by the characteristic value of R_L in the Langmuir isotherm (R_L= 0.017). It exhibits pseudo-second-order adsorption kinetics and follows the Langmuir adsorption isotherm. The various parameters for the adsorption were studied. The additional specific surface area in SNPs after adsorption is attributed to the presence of Cu(II) ions on the surface. The XPS analysis of the SNPs-Cu composite confirms the interaction of Cu(II) with the surface sulfonic functional group. This weak electrostatic interaction keeps the Cu(II) ions on the surface of SNPs. The optimal values of different parameters were: initial concentration of Cu(II) ion 15 mg/mL, pH 5, and SNPs dosage 25 mg/mL, resulting in the maximum Cu(II) ion removal of 93% from the suspension. The R_L value of the adsorption process is close to zero, indicating its irreversibility. The biosorption of Cu with the abundantly found SNPs is an economical and eco-friendly process. The results may benefit industrial wastewater treatment. The advantage of this process is that it does not require any functionalization of biosorbent. The robust method produced the functionalized biosorbent to remove Cu(II) ions with an effective separation of 93% from the suspension. The maximum value of Cu(II) ions separated from the solution was 43 mg/g of SNPs.

ACKNOWLEDGEMENTS

The authors would like to acknowledge this research work to the Department of Science and Technology, Technology Mission Division, Government of India, for providing financial assistance through the grant number DST/TMD/EWO/2K19/EWFH/2019/111(C).

References

[1] A. Fernandes, P. Makoś, G. Boczkaj, Treatment of bitumen post oxidative effluents by sulfate radicals based advanced oxidation processes (S-AOPs) under alkaline pH conditions, J. Clean. Prod. 195 (2018) 374–384. https://doi.org/10.1016/j.jclepro.2018.05.207.

[2] A. Fernandes, P. Makoś, J.A. Khan, G. Boczkaj, Pilot scale degradation study of 16 selected volatile organic compounds by hydroxyl and sulfate radical based advanced oxidation processes, J. Clean. Prod. 208 (2019) 54–64. https://doi.org/10.1016/j.jclepro.2018.10.081.

[3] A. Fernandes, P. Makoś, Z. Wang, G. Boczkaj, Synergistic effect of TiO2 photocatalytic advanced oxidation processes in the treatment of refinery effluents, Chem. Eng. J. 391 (2020). https://doi.org/10.1016/j.cej.2019.123488.

[4] A. Fernandes, M. Gągol, P. Makos, J.A. Khan, G. Boczkaj, Integrated photocatalytic advanced oxidation system (TiO2/UV/O3/H2O2)for degradation of volatile organic compounds, Sep. Purif. Technol. 224 (2019) 1–14. https://doi.org/10.1016/j.seppur.2019.05.012.

[5] X. Zhang, Y. Liu, Concurrent removal of Cu(II), Co(II) and Ni(II) from wastewater by nanostructured layered sodium vanadosilicate: Competitive adsorption kinetics and mechanisms, J. Environ. Chem. Eng. 9 (2021) 105945. https://doi.org/10.1016/j.jece.2021.105945.

[6] M. Eloussaief, M. Benzina, Efficiency of natural and acid-activated clays in the removal of Pb(II) from aqueous solutions, J. Hazard. Mater. 178 (2010) 753–757. https://doi.org/10.1016/j.jhazmat.2010.02.004.

[7] Y. Fu, L. Wang, W. Peng, Q. Fan, Q. Li, Y. Dong, Y. Liu, G. Boczkaj, Z. Wang, Enabling simultaneous redox transformation of toxic chromium(VI) and arsenic(III) in aqueous media—A review, J. Hazard. Mater. 417 (2021). https://doi.org/10.1016/j.jhazmat.2021.126041.

[8] T.A. Khan, V.V. Singh, Removal of cadmium(II), lead(II), and chromium(VI) ions from aqueous solution using clay, Toxicol. Environ. Chem. 92 (2010) 1435–1446. https://doi.org/10.1080/02772241003592930.

[9] S. De Gisi, G. Lofrano, M. Grassi, M. Notarnicola, Characteristics and adsorption

capacities of low-cost sorbents for wastewater treatment: A review, Sustain. Mater. Technol. 9 (2016) 10–40. https://doi.org/10.1016/j.susmat.2016.06.002.

[10] O.D. Kochkodan, V.M. Kochkodan, V.K. Sharma, Removal of Cu(II) in water by polymer enhanced ultrafiltration: Influence of polymer nature and pH, J. Environ. Sci. Heal. Part A. 53 (2018) 33–38. https://doi.org/10.1080/10934529.2017.1366240.

[11] T. Wang, Y. Cao, G. Qu, Q. Sun, T. Xia, X. Guo, H. Jia, L. Zhu, Novel Cu(II)–EDTA Decomplexation by Discharge Plasma Oxidation and Coupled Cu Removal by Alkaline Precipitation: Underneath Mechanisms, Environ. Sci. Technol. 52 (2018) 7884–7891. https://doi.org/10.1021/acs.est.8b02039.

[12] X. Wang, Z. Wang, H. Chen, Z. Wu, Removal of Cu(II) ions from contaminated waters using a conducting microfiltration membrane, J. Hazard. Mater. 339 (2017) 182–190. https://doi.org/10.1016/j.jhazmat.2017.06.038.

[13] E.A. Abdelrahman, Y.G. Abou El-Reash, H.M. Youssef, Y.H. Kotp, R.M. Hegazey, Utilization of rice husk and waste aluminum cans for the synthesis of some nanosized zeolite, zeolite/zeolite, and geopolymer/zeolite products for the efficient removal of Co(II), Cu(II), and Zn(II) ions from aqueous media, J. Hazard. Mater. 401 (2021) 123813. https://doi.org/10.1016/j.jhazmat.2020.123813.

[14] M. Gholizadeh, X. Hu, Removal of heavy metals from soil with biochar composite: A critical review of the mechanism, J. Environ. Chem. Eng. 9 (2021) 105830. https://doi.org/https://doi.org/10.1016/j.jece.2021.105830.

[15] M.B. Tahir, H. Kiran, T. Iqbal, The detoxification of heavy metals from aqueous environment using nano-photocatalysis approach: a review, Environ. Sci. Pollut. Res. 26 (2019) 10515–10528. https://doi.org/10.1007/s11356-019-04547-x.

[16] D.S. Malik, C.K. Jain, A.K. Yadav, Removal of heavy metals from emerging cellulosic low-cost adsorbents: a review, Appl. Water Sci. 7 (2017) 2113–2136. https://doi.org/10.1007/s13201-016-0401-8.

[17] A. Celekli, B. Bozkus, H. Bozkurt, Development of a new adsorbent from pumpkin husk by KOH-modification to remove copper ions, Environ. Sci. Pollut. Res. 26 (2019) 11514–11523. https://doi.org/10.1007/s11356-017-1160-2.

[18] R. Slimani, I. El Ouahabi, A. Elmchaouri, B. Cagnon, S. El Antri, S. Lazar, Adsorption of copper (II) and zinc (II) onto calcined animal bone meal. Part I: Kinetic and

thermodynamic parameters, Chem. Data Collect. 9–10 (2017) 184–196. https://doi.org/10.1016/j.cdc.2017.06.006.

[19] M. qin Jiang, X. ying Jin, X.Q. Lu, Z. liang Chen, Adsorption of Pb(II), Cd(II), Ni(II) and Cu(II) onto natural kaolinite clay, Desalination. 252 (2010) 33–39. https://doi.org/10.1016/j.desal.2009.11.005.

[20] J. El-Gaayda, F.E. Titchou, R. Oukhrib, P.-S. Yap, T. Liu, M. Hamdani, R. Ait Akbour, Natural flocculants for the treatment of wastewaters containing dyes or heavy metals: A state-of-the-art review, J. Environ. Chem. Eng. 9 (2021) 106060. https://doi.org/https://doi.org/10.1016/j.jece.2021.106060.

[21] M.A. Shaida, R.K. Dutta, A.K. Sen, S.S. Ram, M. Sudarshan, M. Naushad, G. Boczkaj, M.S. Nawab, Chemical analysis of low carbon content coals and their applications as dye adsorbent, Chemosphere. 287 (2022) 132286. https://doi.org/https://doi.org/10.1016/j.chemosphere.2021.132286.

[22] S.T. Neeli, H. Ramsurn, C.Y. Ng, Y. Wang, J. Lu, Removal of Cr (VI), As (V), Cu (II), and Pb (II) using cellulose biochar supported iron nanoparticles: A kinetic and mechanistic study, J. Environ. Chem. Eng. 8 (2020) 103886. https://doi.org/10.1016/j.jece.2020.103886.

[23] A. Tripathi, M. Rawat Ranjan, Heavy Metal Removal from Wastewater Using Low Cost Adsorbents, J. Bioremediation Biodegrad. 06 (2015). https://doi.org/10.4172/2155-6199.1000315.

[24] M.E. Argun, S. Dursun, A new approach to modification of natural adsorbent for heavy metal adsorption, Bioresour. Technol. 99 (2008) 2516–2527. https://doi.org/10.1016/j.biortech.2007.04.037.

[25] X. Wang, Y. Guo, L. Yang, M. Han, J. Zhao, X. Cheng, Nanomaterials as Sorbents to Remove Heavy Metal Ions in Wastewater Treatment, J. Environ. Anal. Toxicol. 02 (2012). https://doi.org/10.4172/2161-0525.1000154.

[26] H. Sadegh, G.A.M. Ali, V.K. Gupta, A.S.H. Makhlouf, R. Shahryari-ghoshekandi, M.N. Nadagouda, M. Sillanpää, E. Megiel, The role of nanomaterials as effective adsorbents and their applications in wastewater treatment, J. Nanostructure Chem. 7 (2017) 1–14. https://doi.org/10.1007/s40097-017-0219-4.

[27] Y. He, W. Xiao, G. Li, F. Yang, P. Wu, T. Yang, C. Chen, P. Ding, A novel lead-ion-

imprinted magnetic biosorbent: preparation, optimization and characterization, Environ. Technol. (United Kingdom). 40 (2019) 499–507. https://doi.org/10.1080/09593330.2017.1397762.

[28] K. Kumar, S.S. Patavardhan, S. Lobo, R. Gonsalves, Equilibrium study of dried orange peel for its efficiency in removal of cupric ions from water, Int. J. Phytoremediation. 20 (2018) 593–598. https://doi.org/10.1080/15226514.2017.1405379.

[29] S. Wang, S. Zhong, X. Zheng, D. Xiao, L. Zheng, Y. Yang, H. Zhang, B. Ai, Z. Sheng, Calcite modification of agricultural waste biochar highly improves the adsorption of Cu(II) from aqueous solutions, J. Environ. Chem. Eng. 9 (2021) 106215. https://doi.org/10.1016/j.jece.2021.106215.

[30] E.K. Guechi, O. Hamdaoui, Evaluation of potato peel as a novel adsorbent for the removal of Cu(II) from aqueous solutions: equilibrium, kinetic, and thermodynamic studies, Desalin. Water Treat. 57 (2016) 10677–10688. https://doi.org/10.1080/19443994.2015.1038739.

[31] L. Darmayanti, S. Notodarmodjo, E. Damanhuri, Removal of copper (II) ions in aqueous solutions by sorption onto fly ash, J. Eng. Technol. Sci. 49 (2017) 546–559. https://doi.org/10.5614/j.eng.technol.sci.2017.49.4.9.

[32] J. Bayuo, K.B. Pelig-Ba, M.A. Abukari, Adsorptive removal of chromium(VI) from aqueous solution unto groundnut shell, Appl. Water Sci. 9 (2019) 1–11. https://doi.org/10.1007/s13201-019-0987-8.

[33] J.H. Park, Y.S. Ok, S.H. Kim, J.S. Cho, J.S. Heo, R.D. Delaune, D.C. Seo, Competitive adsorption of heavy metals onto sesame straw biochar in aqueous solutions, Chemosphere. 142 (2016) 77–83. https://doi.org/10.1016/j.chemosphere.2015.05.093.

[34] G.V.S.R. Pavan Kumar, K.A. Malla, B. Yerra, K. Srinivasa Rao, Removal of Cu(II) using three low-cost adsorbents and prediction of adsorption using artificial neural networks, Appl. Water Sci. 9 (2019) 1–9. https://doi.org/10.1007/s13201-019-0924-x.

[35] L.M. Pandey, Surface engineering of nano-sorbents for the removal of heavy metals: Interfacial aspects, J. Environ. Chem. Eng. 9 (2021) 104586. https://doi.org/https://doi.org/10.1016/j.jece.2020.104586.

[36] M.R. Awual, G.E. Eldesoky, T. Yaita, M. Naushad, H. Shiwaku, Z.A. AlOthman, S. Suzuki, Schiff based ligand containing nanocomposite adsorbent for optical copper(II)

ions removal from aqueous solutions, Chem. Eng. J. 279 (2015) 639–647. https://doi.org/10.1016/j.cej.2015.05.049.

[37] O.A. Oyetade, V.O. Nyamori, B.S. Martincigh, S.B. Jonnalagadda, Nitrogen-functionalised carbon nanotubes as a novel adsorbent for the removal of Cu(ii) from aqueous solution, RSC Adv. 6 (2016) 2731–2745. https://doi.org/10.1039/c5ra23900a.

[38] F. Zhao, E. Repo, D. Yin, M.E.T. Sillanpaa, Adsorption of Cd(II) and Pb(II) by a novel EGTA-modified chitosan material: Kinetics and isotherms, J. Colloid Interface Sci. 409 (2013) 174–182. https://doi.org/10.1016/j.jcis.2013.07.062.

[39] M.A. Renu, K. Singh, S. Upadhyaya, R.K. Dohare, Removal of heavy metals from wastewater using modified agricultural adsorbents, Mater. Today Proc. 4 (2017) 10534–10538. https://doi.org/10.1016/j.matpr.2017.06.415.

[40] O.E. Abdel Salam, N.A. Reiad, M.M. ElShafei, A study of the removal characteristics of heavy metals from wastewater by low-cost adsorbents, J. Adv. Res. 2 (2011) 297–303. https://doi.org/10.1016/j.jare.2011.01.008.

[41] M. Perez Herrera, T. Vasanthan, R. Hoover, Characterization of Maize Starch Nanoparticles Prepared by Acid Hydrolysis, Cereal Chem. 93 (2016) 323–330. https://doi.org/10.1094/CCHEM-08-15-0175-R.

[42] S. Wang, L. Copeland, Effect of Acid Hydrolysis on Starch Structure and Functionality : A Review, Crit. Rev. Food Sci. Nutr. 55 (2015) 1081–1097. https://doi.org/10.1080/10408398.2012.684551.

[43] S. Shabana, R. Prasansha, I. Kalinina, I. Potoroko, U. Bagale, S.H. Shirish, Ultrasound assisted acid hydrolyzed structure modification and loading of antioxidants on potato starch nanoparticles, Ultrason. Sonochem. 51 (2019) 444–450. https://doi.org/10.1016/j.ultsonch.2018.07.023.

[44] S. Bel Haaj, A. Magnin, C. Petrier, S. Boufi, Starch nanoparticles formation via high power ultrasonication, Carbohydr. Polym. 92 (2013) 1625–1632. https://doi.org/10.1016/j.carbpol.2012.11.022.

[45] N. Masina, Y.E. Choonara, P. Kumar, L.C. du Toit, M. Govender, S. Indermun, V. Pillay, A review of the chemical modification techniques of starch, Carbohydr. Polym. 157 (2017) 1226–1236. https://doi.org/10.1016/j.carbpol.2016.09.094.

[46] S. Shrestha, B. Wang, P. Dutta, Nanoparticle processing: Understanding and controlling

aggregation, Adv. Colloid Interface Sci. 279 (2020) 102162. https://doi.org/10.1016/j.cis.2020.102162.

[47] K. Loza, M. Epple, M. Maskos, Stability of nanoparticle dispersions and particle agglomeration, Springer International Publishing, 2019. https://doi.org/10.1007/978-3-030-12461-8_4.

[48] V.S. Hakke, U.D. Bagale, S. Boufi, G.U.B. Babu, S.H. Sonawane, Ultrasound Assisted Synthesis of Starch Nanocrystals and It's Applications with Polyurethane for Packaging Film, J. Renew. Mater. 08 (2020) 239–250. https://doi.org/10.32604/jrm.2020.08449.

[49] S.F. Chin, S.C. Pang, S.H. Tay, Size controlled synthesis of starch nanoparticles by a simple nanoprecipitation method, Carbohydr. Polym. 86 (2011) 1817–1819. https://doi.org/10.1016/j.carbpol.2011.07.012.

[50] L. Brinza, K. Geraki, I.G. Breaban, M. Neamtu, Zn adsorption onto Irish Fucus vesiculosus: Biosorbent uptake capacity and atomistic mechanism insights, J. Hazard. Mater. 365 (2019) 252–260. https://doi.org/10.1016/j.jhazmat.2018.11.009.

[51] K.T. Kubra, M.S. Salman, M.N. Hasan, A. Islam, M.M. Hasan, M.R. Awual, Utilizing an alternative composite material for effective copper(II) ion capturing from wastewater, J. Mol. Liq. 336 (2021) 116325. https://doi.org/10.1016/j.molliq.2021.116325.

[52] D. Bozic, M. Gorgievski, V. Stankovic, N. Strbac, S. Serbula, N. Petrovic, Adsorption of heavy metal ions by beech sawdust - Kinetics, mechanism and equilibrium of the process, Ecol. Eng. 58 (2013) 202–206. https://doi.org/10.1016/j.ecoleng.2013.06.033.

[53] S. Muthusaravanan, N. Sivarajasekar, J.S. Vivek, T. Paramasivan, M. Naushad, J. Prakashmaran, V. Gayathri, O.K. Al-Duaij, Phytoremediation of heavy metals: mechanisms, methods and enhancements, Environ. Chem. Lett. 16 (2018) 1339–1359. https://doi.org/10.1007/s10311-018-0762-3.

[54] B. Singha, S.K. Das, Adsorptive removal of Cu(II) from aqueous solution and industrial effluent using natural/agricultural wastes, Colloids Surfaces B Biointerfaces. 107 (2013) 97–106. https://doi.org/10.1016/j.colsurfb.2013.01.060.

[55] W. Zhang, J. Song, Q. He, H. Wang, W. Lyu, H. Feng, W. Xiong, W. Guo, J. Wu, L. Chen, Novel pectin based composite hydrogel derived from grapefruit peel for enhanced Cu(II) removal, J. Hazard. Mater. 384 (2020) 121445. https://doi.org/10.1016/j.jhazmat.2019.121445.

[56] S. Golshan Shandi, F. Doulati Ardejani, F. Sharifi, Assessment of Cu (II) removal from an aqueous solution by raw Gundelia tournefortii as a new low-cost biosorbent: Experiments and modelling, Chinese J. Chem. Eng. 27 (2019) 1945–1955. https://doi.org/10.1016/j.cjche.2018.12.027.

[57] M.I. Sabela, K. Kunene, S. Kanchi, N.M. Xhakaza, A. Bathinapatla, P. Mdluli, D. Sharma, K. Bisetty, Removal of copper (II) from wastewater using green vegetable waste derived activated carbon: An approach to equilibrium and kinetic study, Arab. J. Chem. 12 (2019) 4331–4339. https://doi.org/10.1016/j.arabjc.2016.06.001.

[58] M. Naushad, A. Mittal, M. Rathore, V. Gupta, Ion-exchange kinetic studies for Cd(II), Co(II), Cu(II), and Pb(II) metal ions over a composite cation exchanger, Desalin. Water Treat. 54 (2015) 2883–2890. https://doi.org/10.1080/19443994.2014.904823.

[59] G.R. Belton, Langmuir adsorption, the Gibbs adsorption isotherm, and interfacial kinetics in liquid metal systems, Metall. Mater. Trans. B. 7 (1976) 35–42. https://doi.org/10.1007/BF02652817.

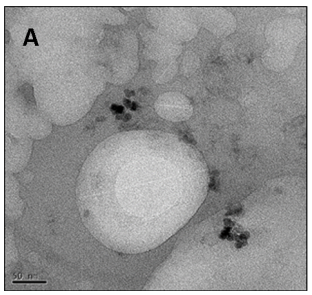

CJCE_24588_CJCE-22-0086.R1_Figure 1A.tif

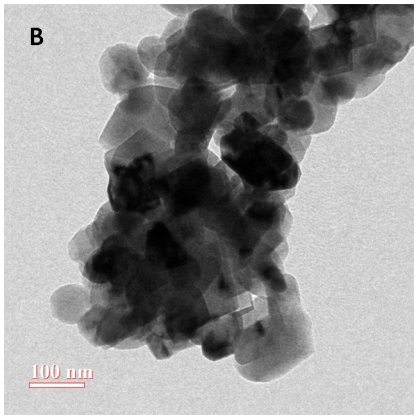

CJCE_24588_CJCE-22-0086.R1_Figure 1B.tif

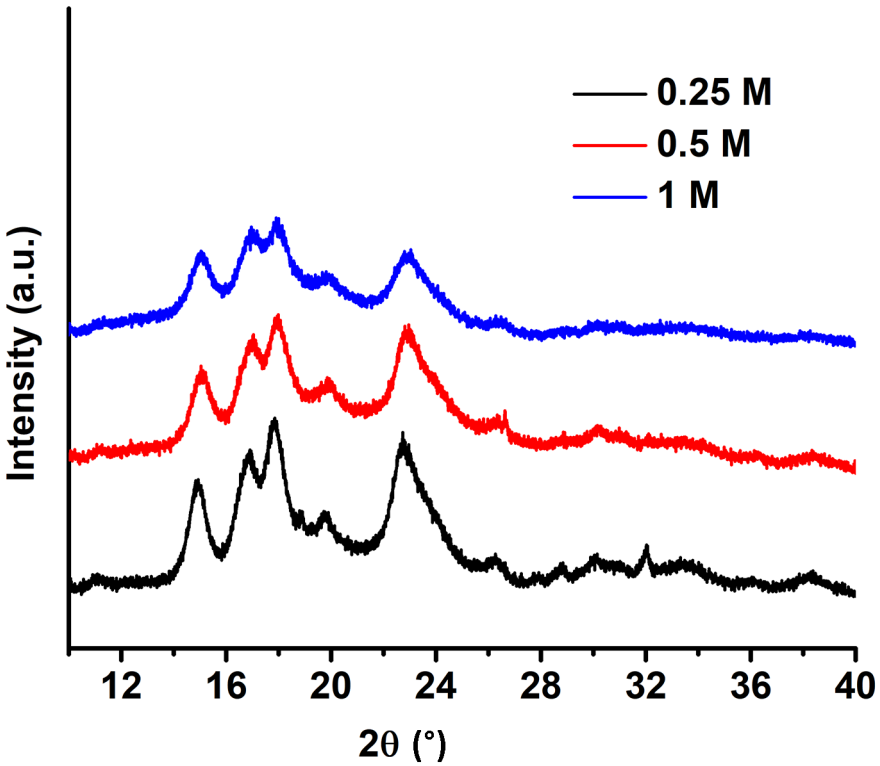

CJCE_24588_CJCE-22-0086.R1_Figure 2.tif

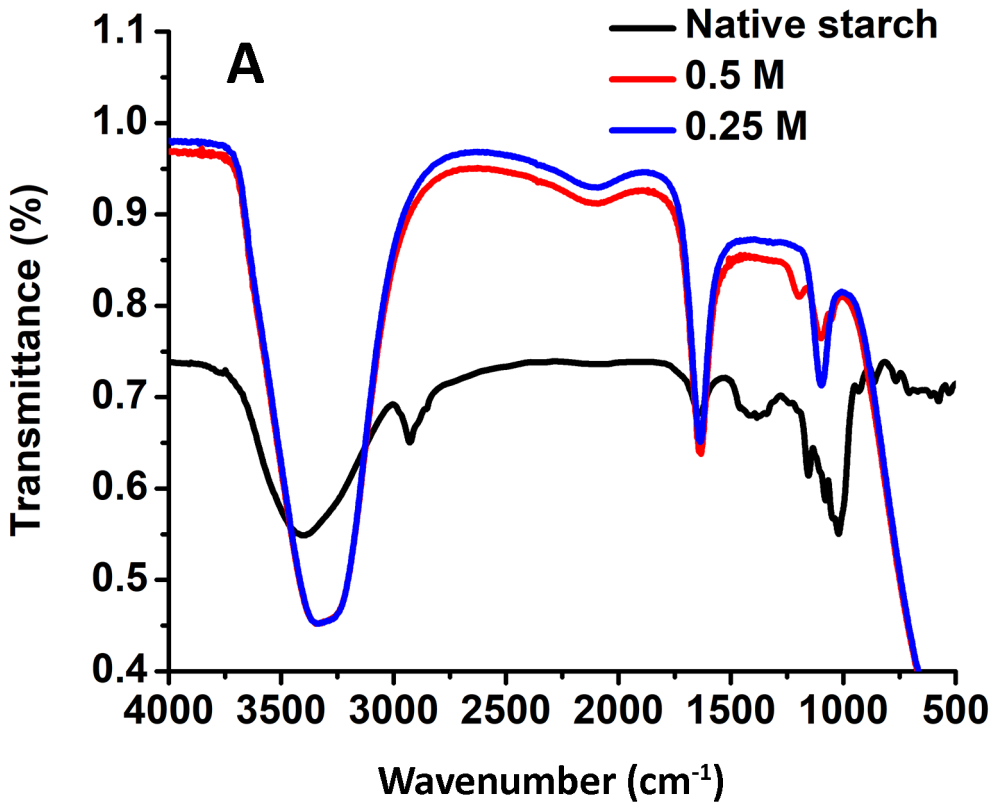

CJCE_24588_CJCE-22-0086.R1_Figure 3A.tif

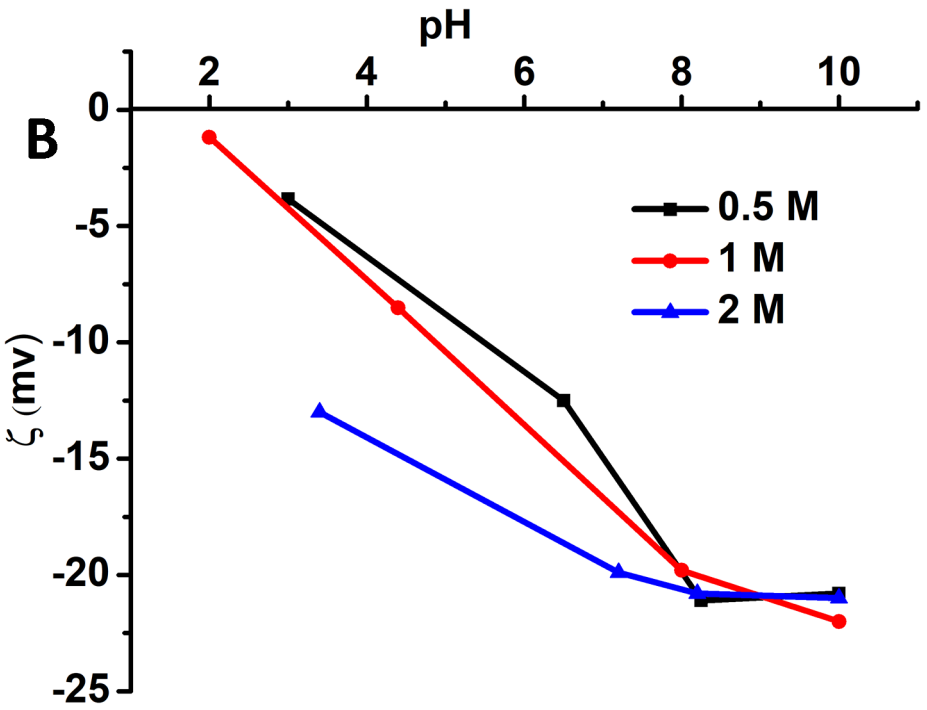

CJCE_24588_CJCE-22-0086.R1_Figure 3B.tif

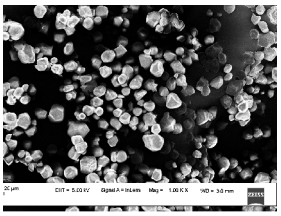

A

CJCE_24588_CJCE-22-0086.R1_Figure 4A.tif

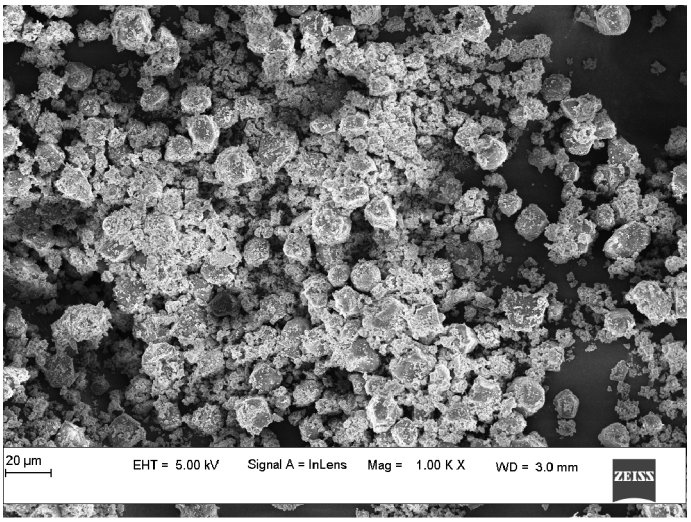

B

CJCE_24588_CJCE-22-0086.R1_Figure 4B.tif

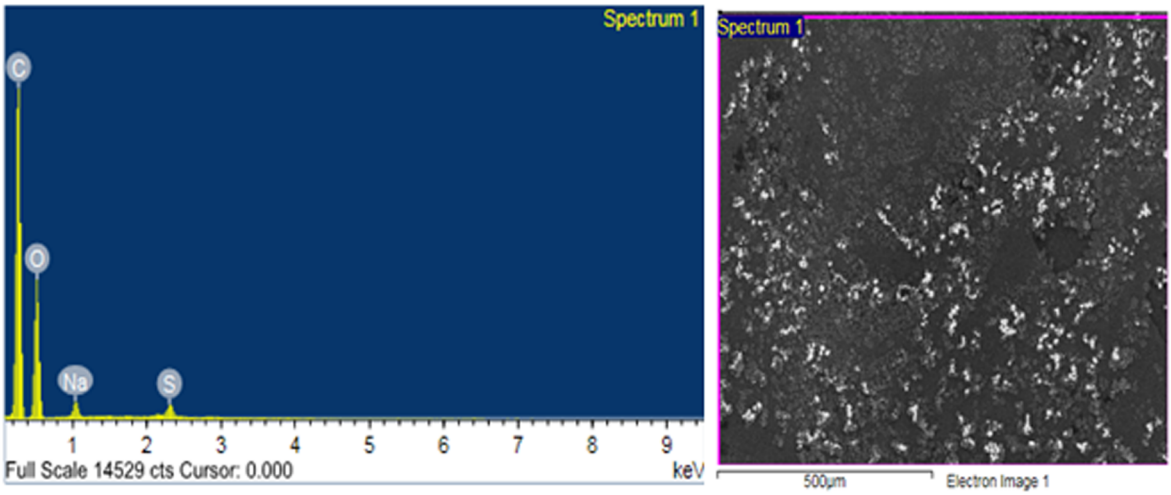

C

CJCE_24588_CJCE-22-0086.R1_Figure 4C.tif

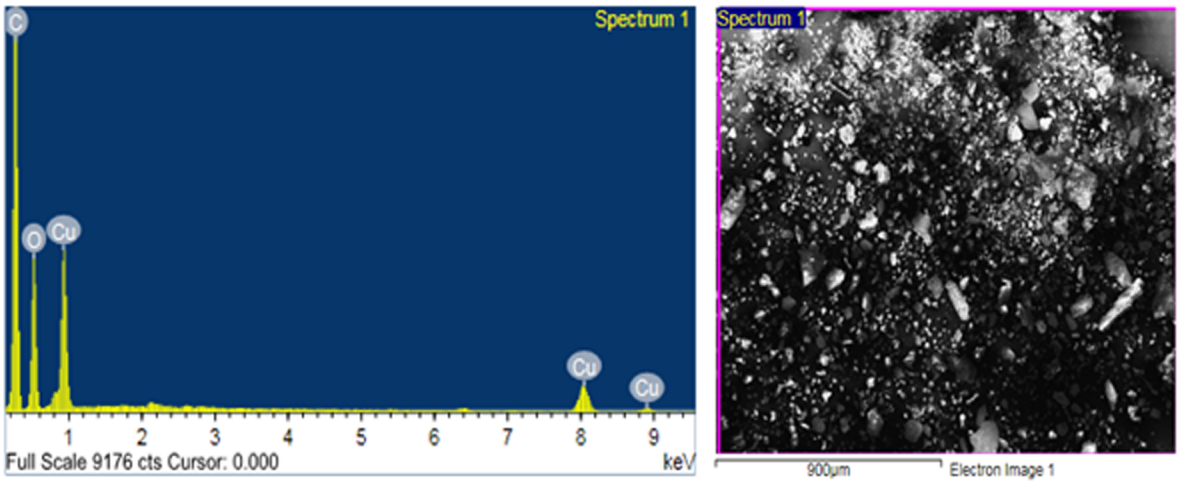

D

CJCE_24588_CJCE-22-0086.R1_Figure 4D.tif

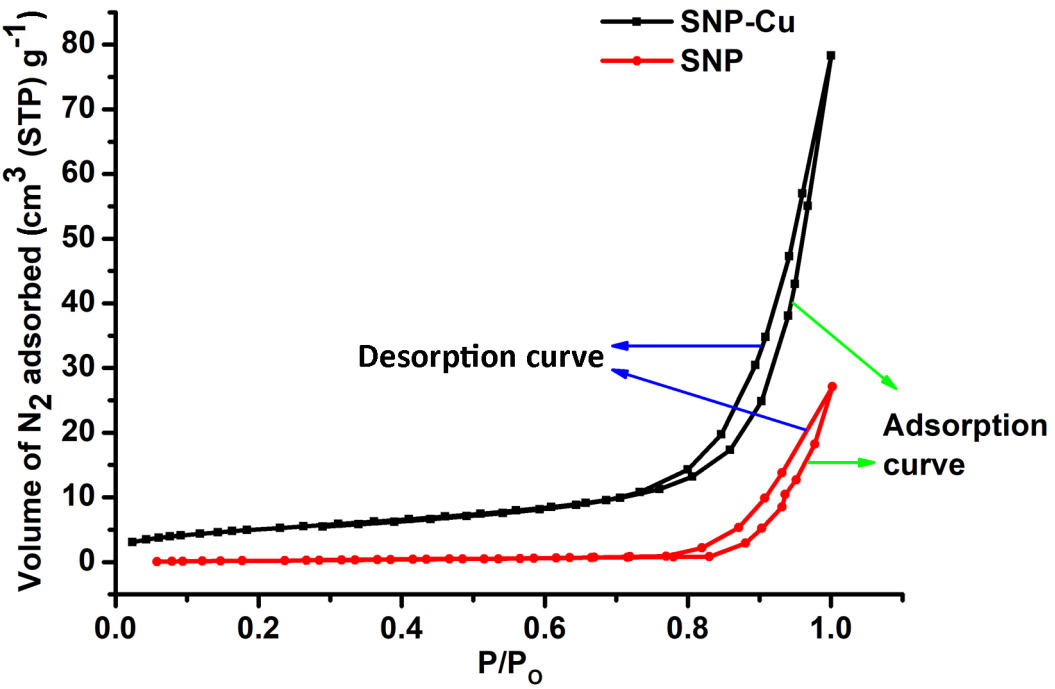

CJCE_24588_CJCE-22-0086.R1_Figure 5.tif

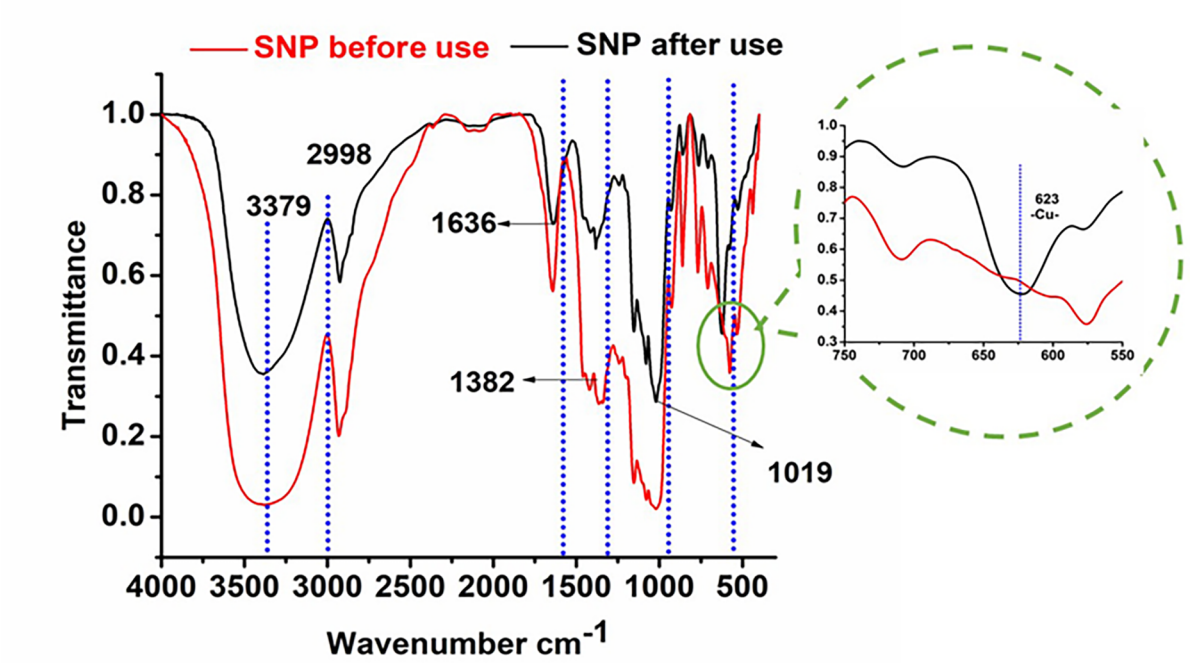

CJCE_24588_CJCE-22-0086.R1_Figure 6.tif

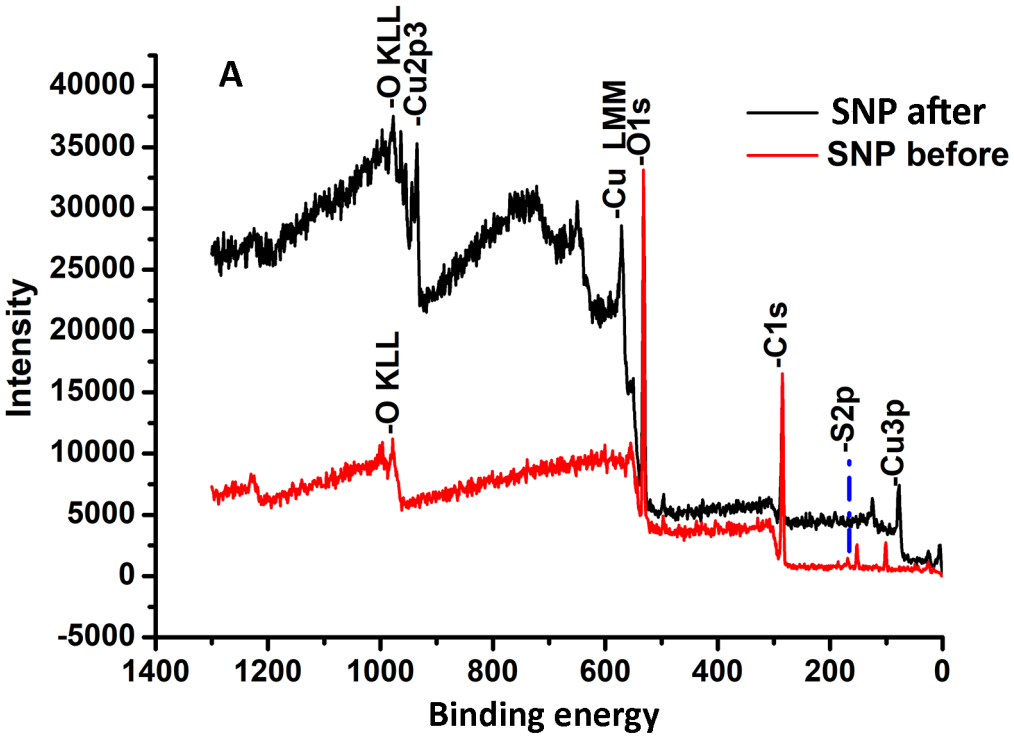

CJCE_24588_CJCE-22-0086.R1_Figure 7A.tif

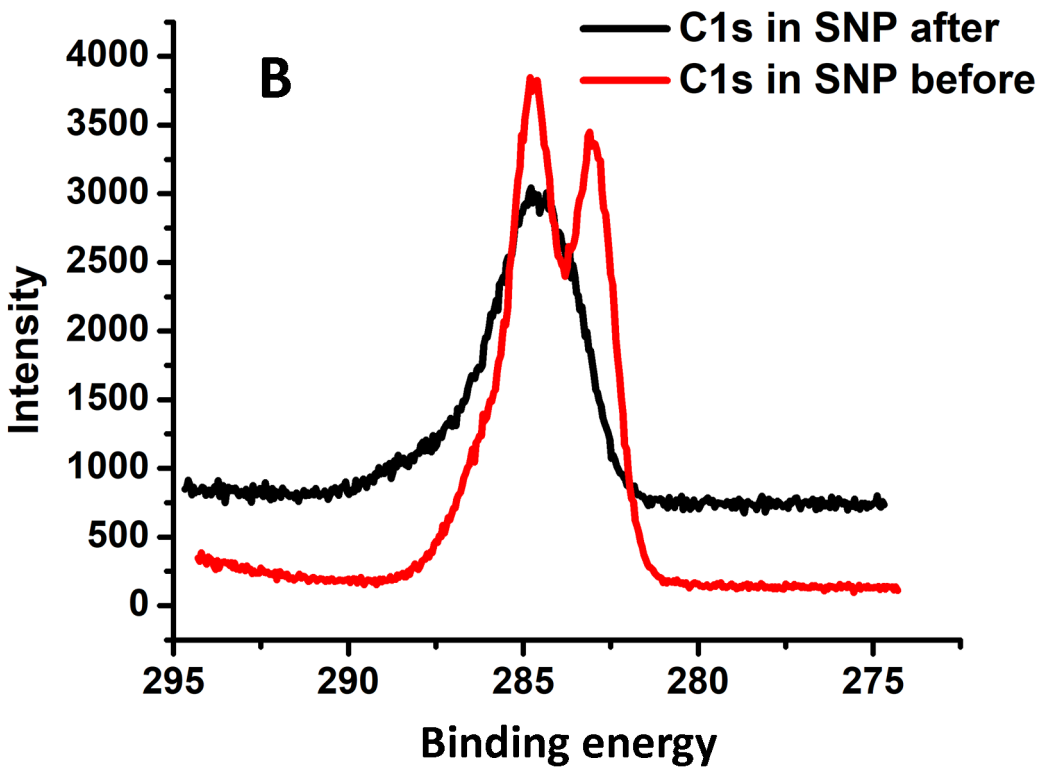

CJCE_24588_CJCE-22-0086.R1_Figure 7B.tif

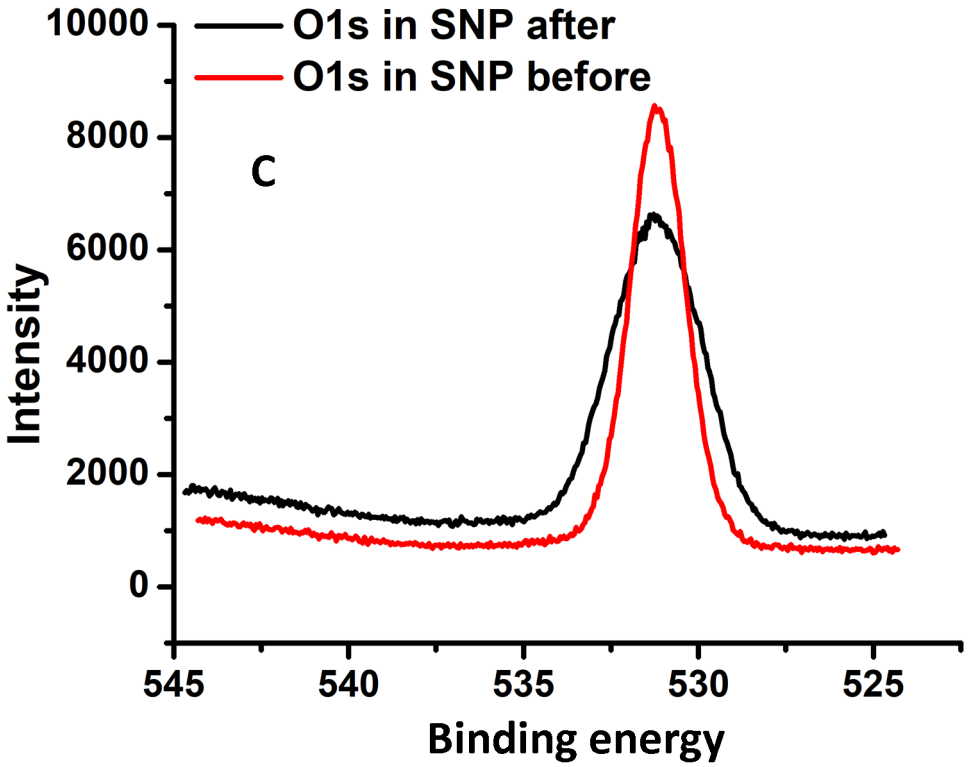

CJCE_24588_CJCE-22-0086.R1_Figure 7C.tif

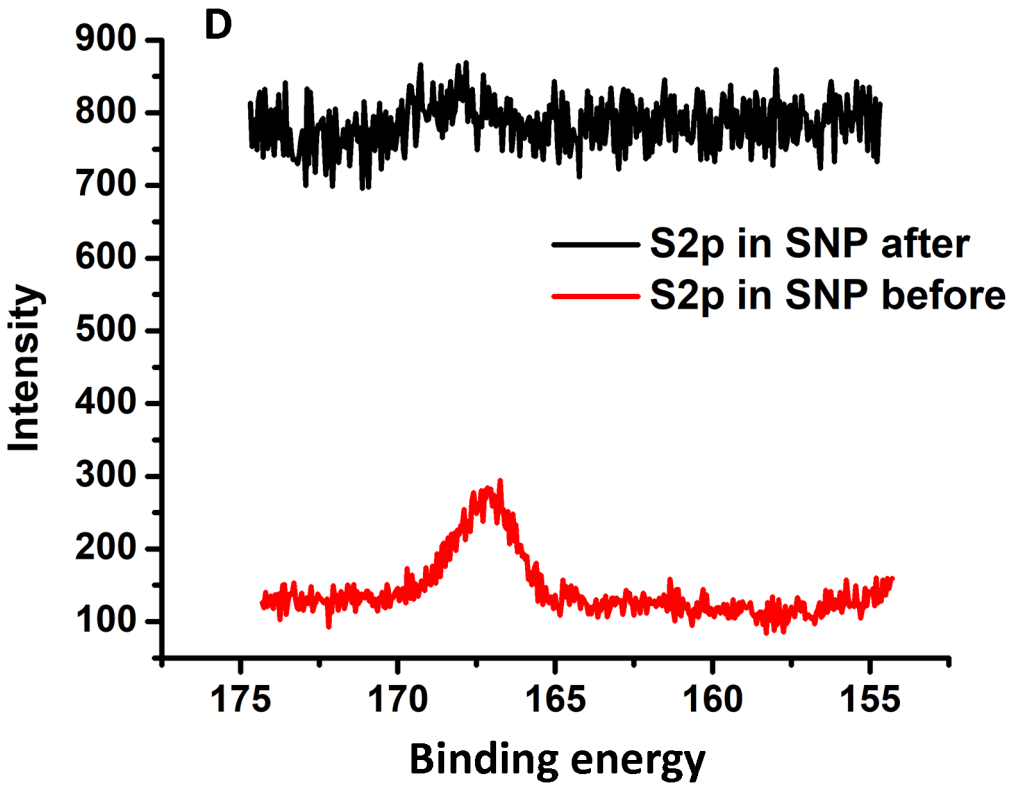

CJCE_24588_CJCE-22-0086.R1_Figure 7D.tif

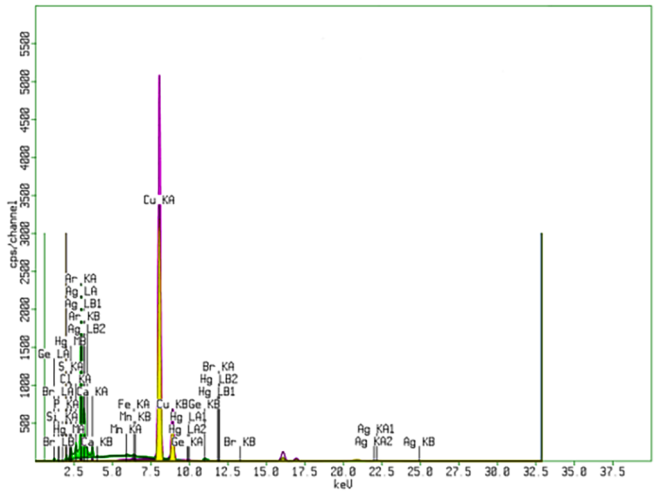

CJCE_24588_CJCE-22-0086.R1_Figure 8.tif

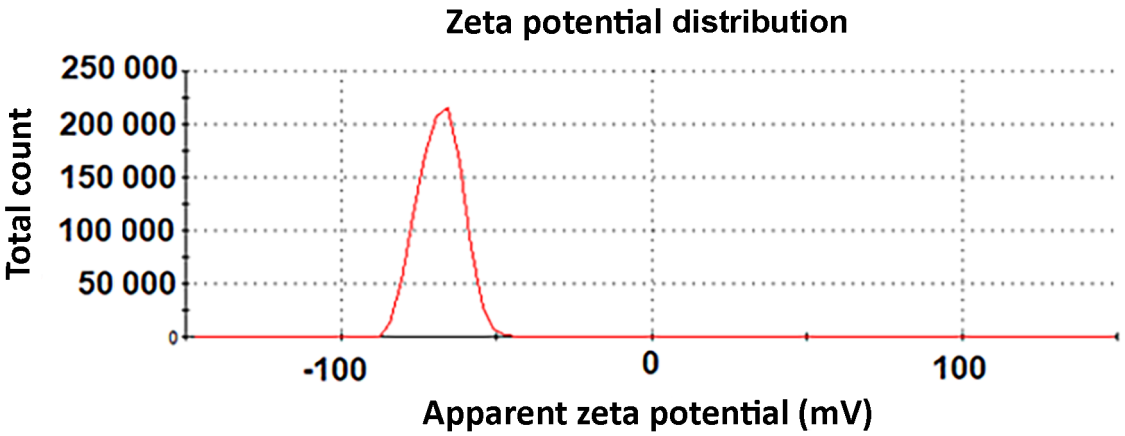

CJCE_24588_CJCE-22-0086.R1_Figure 9.tif

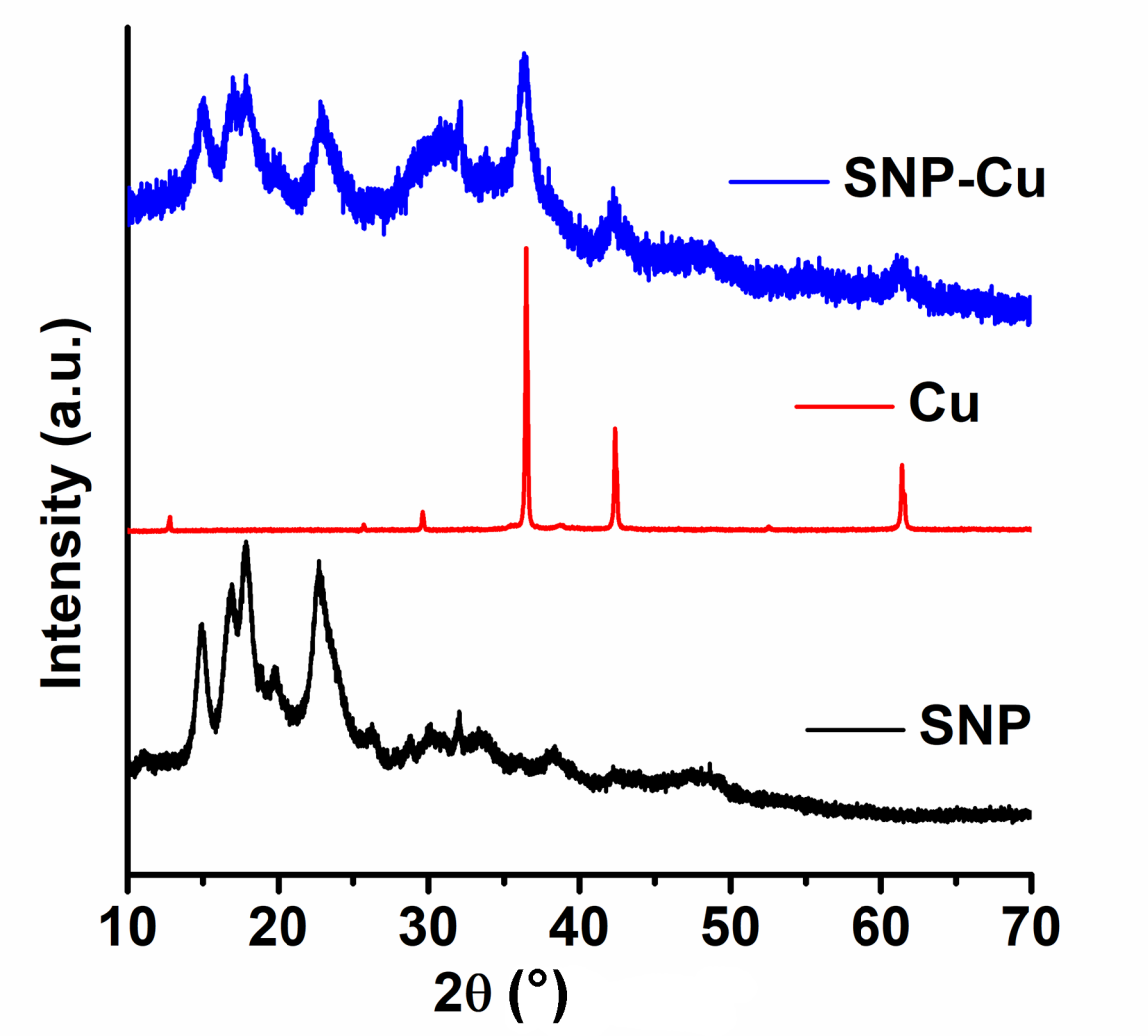

CJCE_24588_CJCE-22-0086.R1_Figure 10.tif

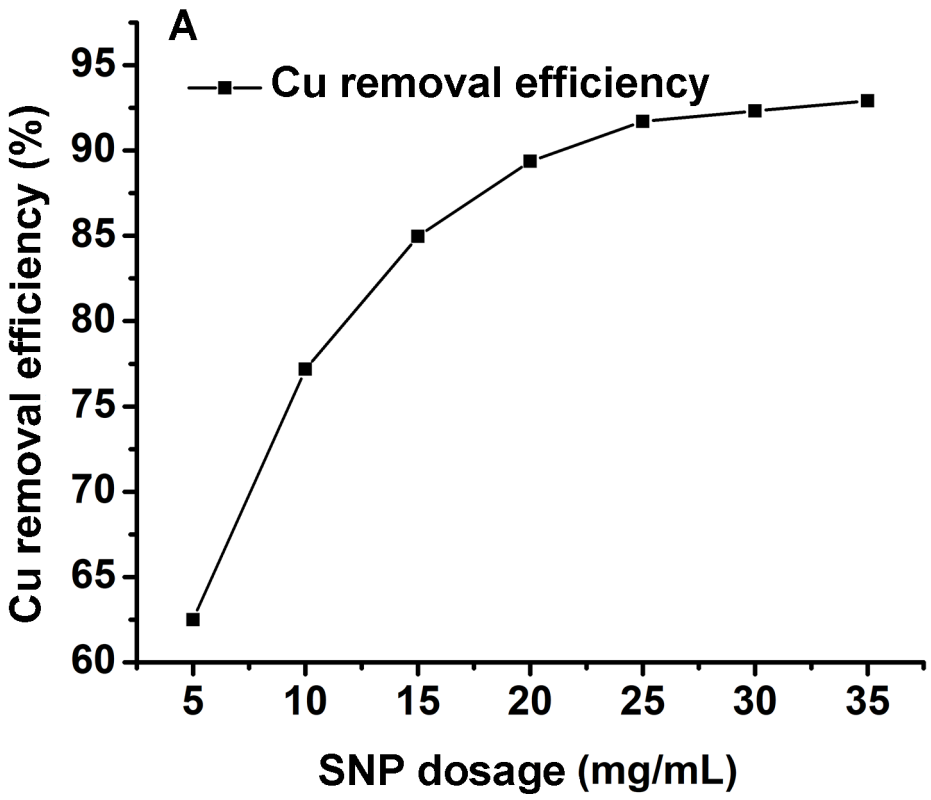

CJCE_24588_CJCE-22-0086.R1_Figure 11A.tif

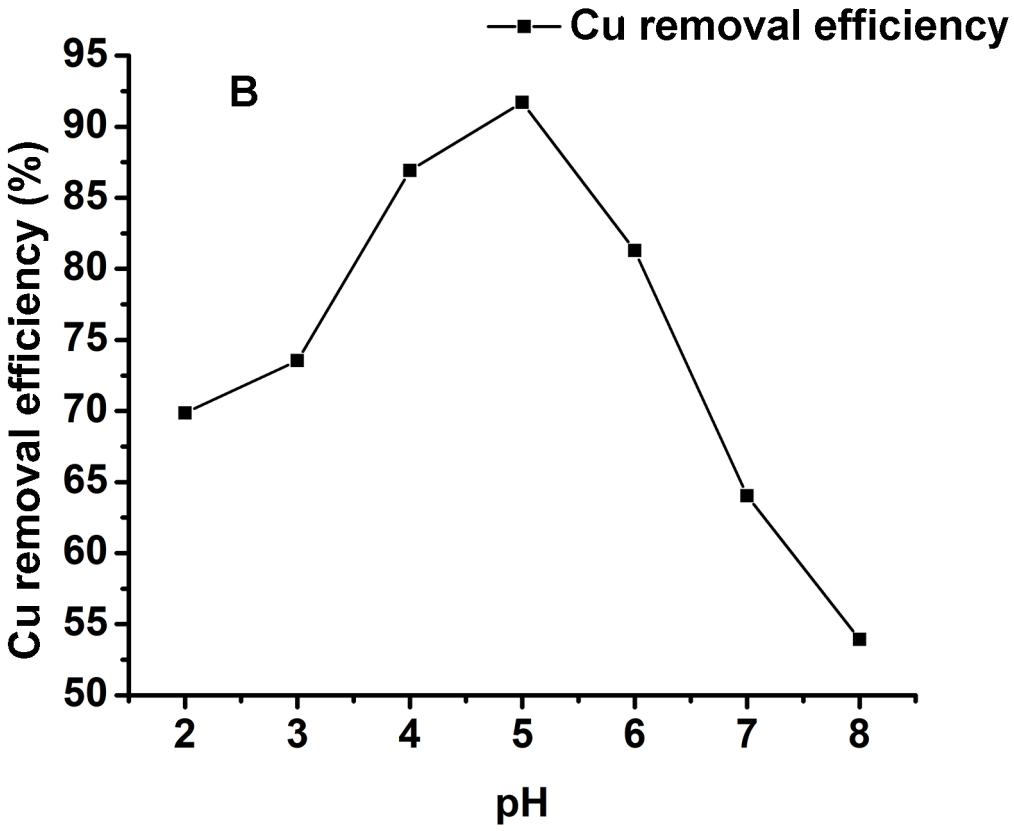

CJCE_24588_CJCE-22-0086.R1_Figure 11B.tif

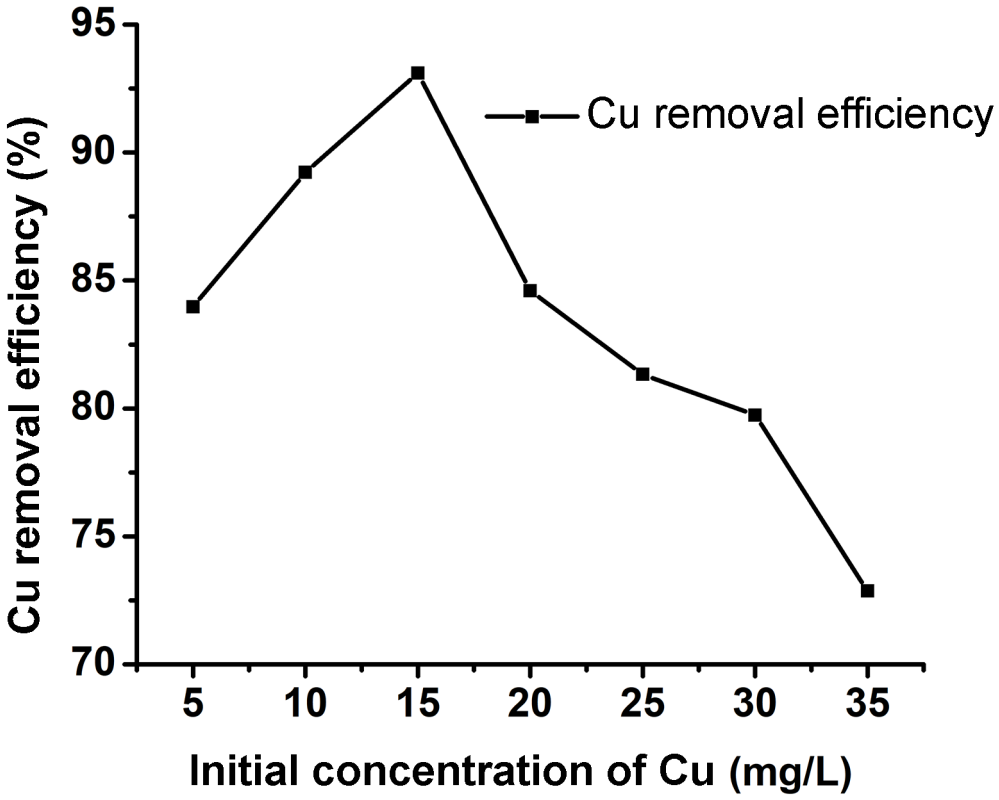

CJCE_24588_CJCE-22-0086.R1_Figure 12.tif

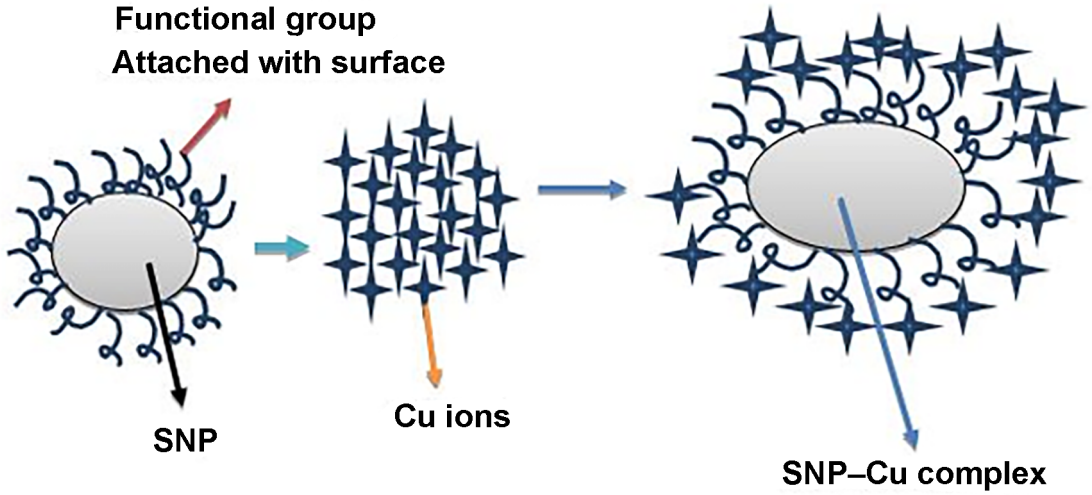

CJCE_24588_CJCE-22-0086.R1_Figure 13.tif

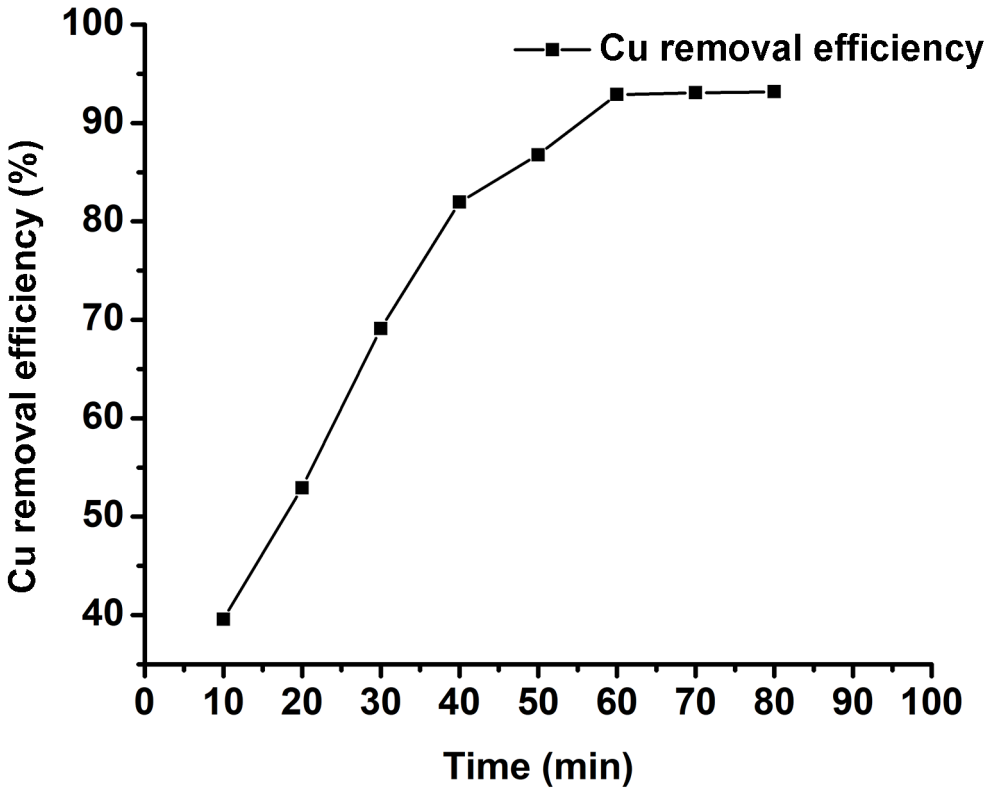

CJCE_24588_CJCE-22-0086.R1_Figure 14.tif

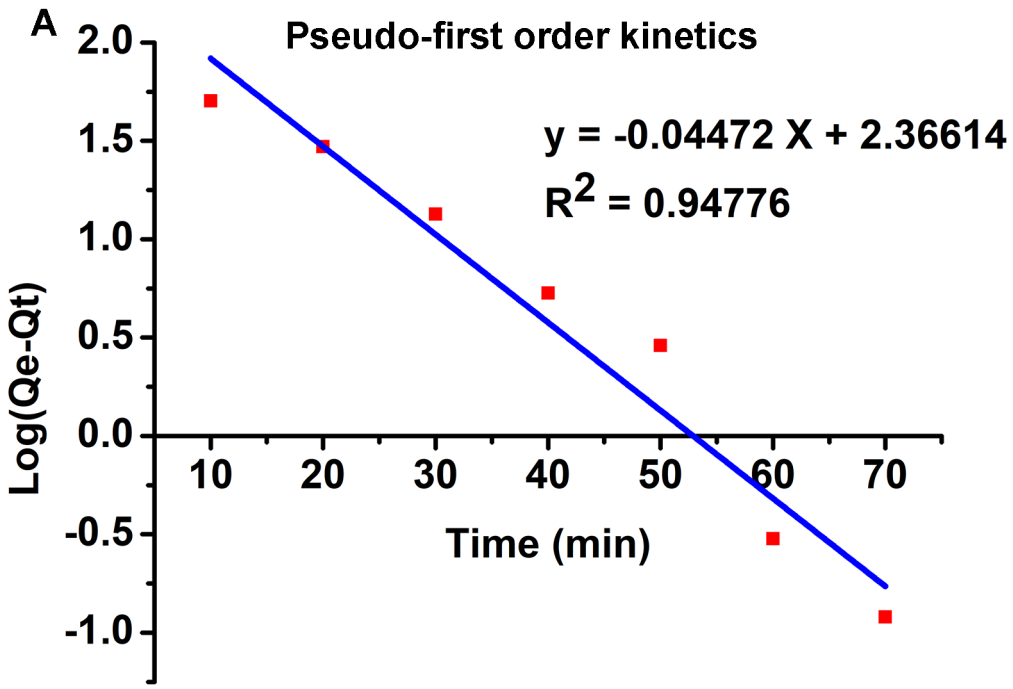

CJCE_24588_CJCE-22-0086.R1_Figure 15A.tif

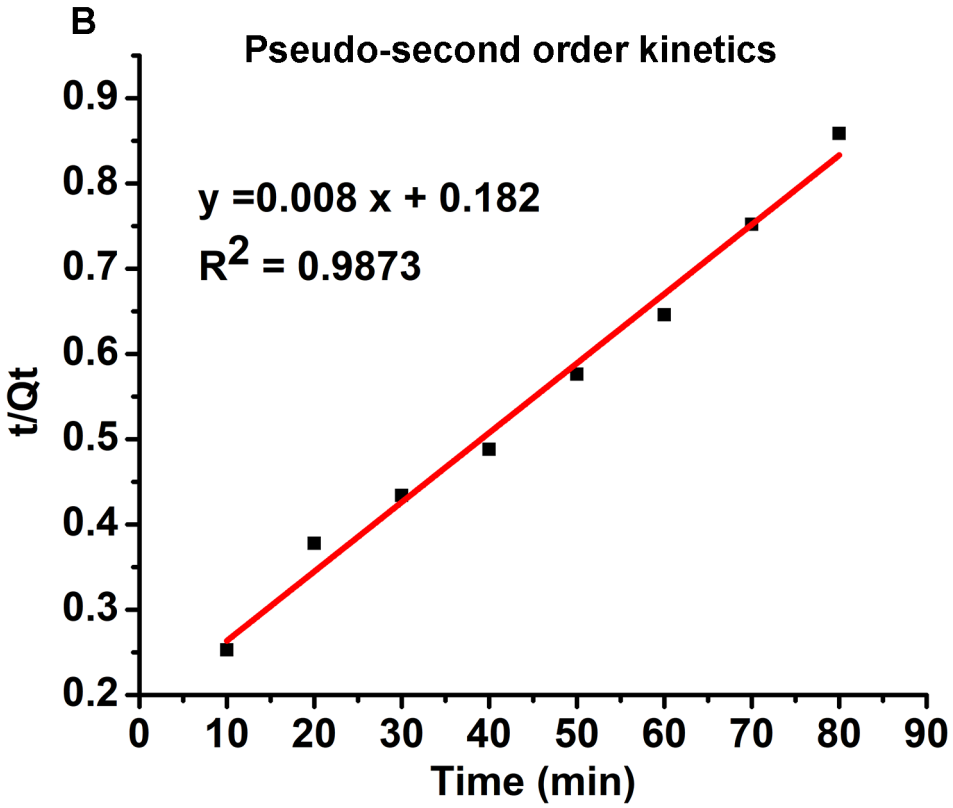

CJCE_24588_CJCE-22-0086.R1_Figure 15B.tif

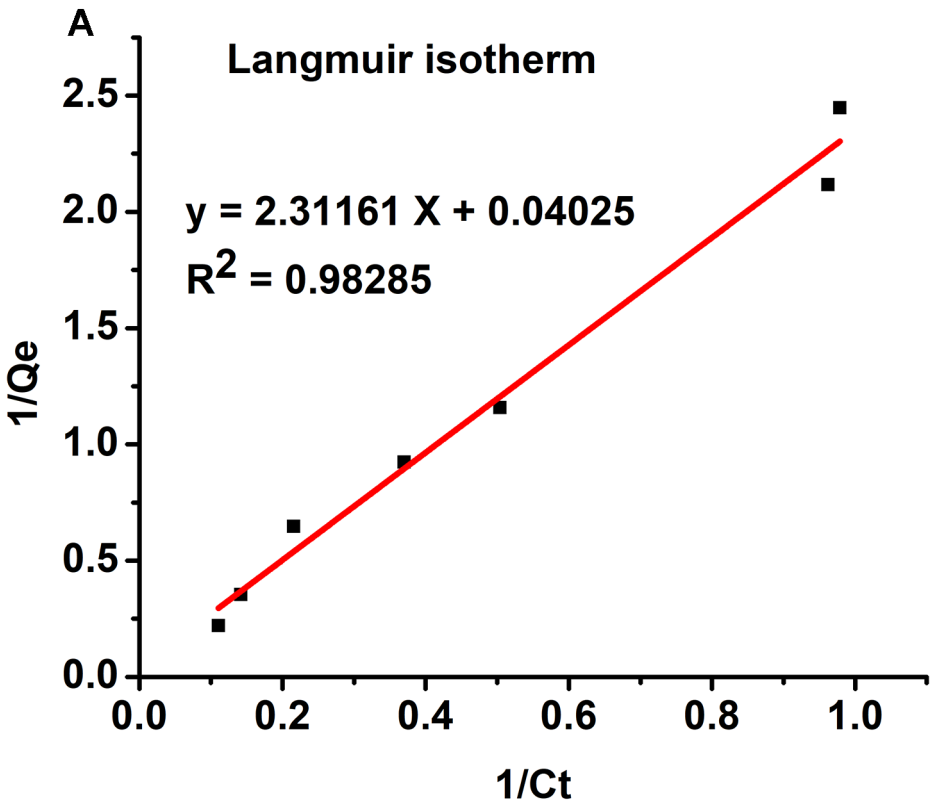

CJCE_24588_CJCE-22-0086.R1_Figure 16A.tif

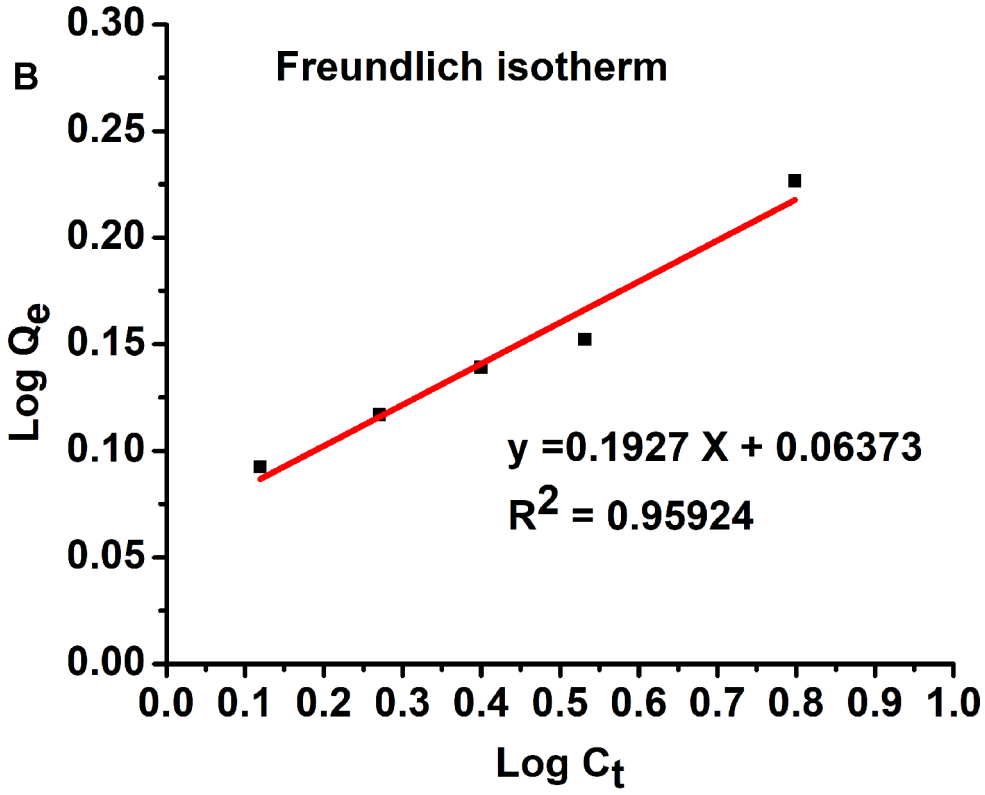

CJCE_24588_CJCE-22-0086.R1_Figure 16B.tif

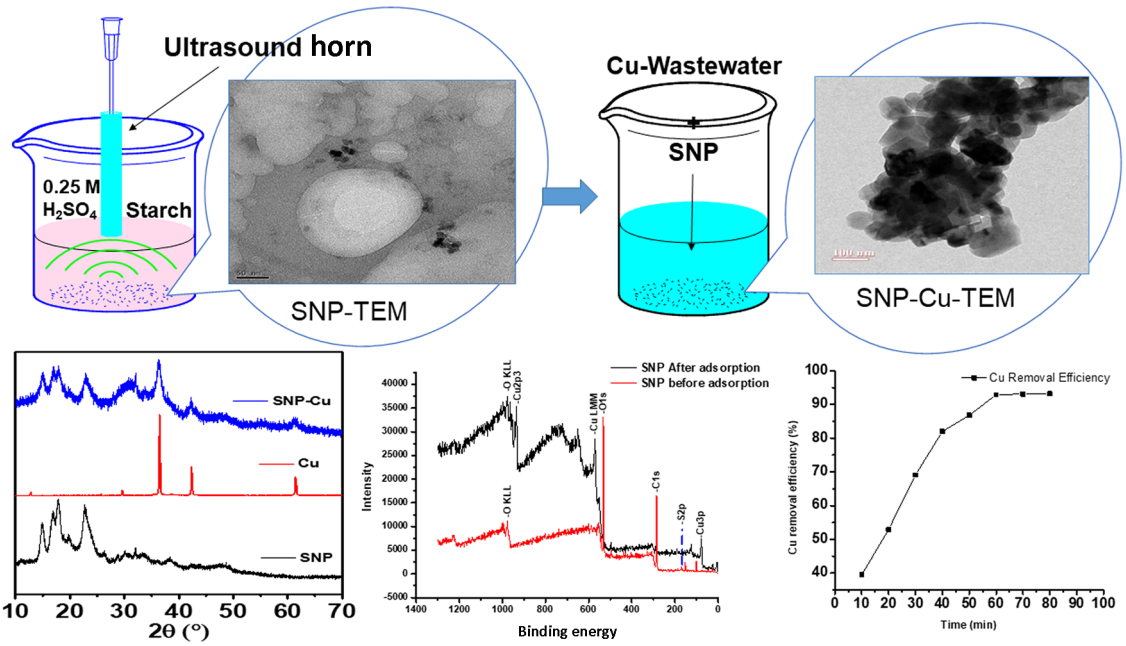

CJCE_24588_CJCE-22-0086.R1_Graphical Abstract.tif